

Rochester Institute of Technology

RIT Digital Institutional Repository

Theses

8-21-2015

Tear Film Dynamics Concerning A Lipid Reservoir

Gregory A. Barron
gab1232@rit.edu

Follow this and additional works at: <https://repository.rit.edu/theses>

Recommended Citation

Barron, Gregory A., "Tear Film Dynamics Concerning A Lipid Reservoir" (2015). Thesis. Rochester Institute of Technology. Accessed from

This Thesis is brought to you for free and open access by the RIT Libraries. For more information, please contact repository@rit.edu.

Tear Film Dynamics Concerning A Lipid Reservoir

by

GREGORY A. BARRON

A Thesis Submitted in Partial Fulfillment of the Requirements
for the Degree of Master of Science in Applied and Computational Mathematics
School of Mathematical Sciences, College of Science

Rochester Institute of Technology

Rochester, NY

August 21, 2015

Committee Approval:



Kara L. Maki, Ph.D. Date
School of Mathematical Sciences
Thesis Advisor

Steven J. Weinstein, Ph.D. Date
The Kate Gleason College of Engineering
Committee Member

Nathaniel S. Barlow, Ph.D. Date
School of Mathematical Sciences
Committee Member

Nathan D. Cahill, D.Phil. Date
School of Mathematical Sciences
Director of Graduate Programs

Abstract

We investigate the dynamics of the human multilayer tear film, subject to a reservoir of lipid at the lids. A numerical method is constructed to solve a one-dimensional tear film model, derived using lubrication theory. Three choices for the open eye boundary conditions are explored including a specified lipid to mimic a lipid reservoir, a no lipid flux boundary condition to conserve lipid initially present in the system, and finally mixed lipid flux boundary condition which to our knowledge, has not been previously studied. For the blinking eye, we choose to use no diffusive flux for the lipid boundary condition.

CONTENTS

I	Introduction	1
II	Literature Review	2
III	One Dimensional Model for the Tear Film Dynamics	5
	III.1 Model Formation	5
	III.2 Nondimensionalization	12
	III.3 Governing Equations for the Tear Film Dynamics	16
IV	Numerical Method	18
V	Numerical Solution - Open Eye	21
	V.1 Study of the Tear Film Dynamics with a Lipid Reservoir at the Lids	22
	V.1.1 Marangoni Effect Turned Off	22
	V.1.2 Marangoni Effect Turned On	26
	V.1.3 Varying the Marangoni Number - Parameter Study	29
	V.2 Study of Tear Film Dynamics with Mixed Boundary Conditions	31
	V.2.1 Mixed Boundary Condition	31
	V.2.2 No Lipid Flux Boundary Condition	34
VI	Numerical Solution - Blinking Eye	37
	VI.1 First Opening Phase	39
	VI.2 Interblink Period	40
	VI.3 Closing Phase	43
	VI.4 Partially Closed Phase	44
	VI.5 Second Opening Phase	45
VII	Discussion	46
	VII.1 Discussion and Conclusion	46
	VII.2 Future Work	47
VIII	Acknowledgment	48
IX	Appendix	48

I. INTRODUCTION

Dry eye is the leading motivation for researching the dynamics of the tear film, as approximately 3.2 million women, and 1.6 million men of age 50 or older suffer from the symptoms of dry eye syndrome in the United States [13]. Incident rates of dry eye are expected to double from the year 2000 to 2050 [13]. Symptoms can include a stinging, burning or scratchy sensation; sensitivity to light; blurred vision; periods of excessive tearing; and a sensation of having a foreign object in your eye. Dry eye is classified as either "aqueous deficient dry eye," where the eye does not produce tears properly or produces tears with improper consistency, or "evaporative dry eye," where the person experiences a quickened evaporation rate [17]. No cure currently exists for dry eye syndrome, and treatments such as the use of eye drops meant to alleviate symptoms have limited affect.

The eye is wet with a multilayer film, referred to as the tear film, consisting of a mucus layer, aqueous layer, and lipid layer in order of appearance from the surface of the eye to the air [12]. The tear film restricts the formation of bacteria, ensures that debris is removed or repelled to protect the surface of the eye, and acts as an optical medium [12]. Between the air and aqueous layer is the lipid layer. Lipid is an oily, insoluble substance that acts as a surfactant, and forms the thinnest of the three layers [7, 12]. Lowering the surface tension of the fluid they rest on, several functions of the lipid layer include the smoothing of the aqueous layer, shielding against debris and skin lipid, and maintaining stability of the tear film [7]. At the lid margins, lipid is supplied to the tear film via the meibomian glands. The aqueous layer is the thickest of the multilayered tear film, consisting of 98% water, and is commonly thought of as tears. A mucus layer covers the eye and emits soluble mucins into the aqueous layer [23]. It was originally thought that the mucus layer was necessary for the tear film to wet the eye [12], however the surface of the eye itself has been found to be hydrophilic [25]. The tear fluid is pinned at the hydrophilic surface on the lid, referred to as the grey line, and reaches a thickness of approximately 60 microns to form the menisci near the lids [18]. Away from the menisci, the tear film lays on top of the cornea and sclera at a thickness of approximately $3\mu\text{m}$ [16]. Volume of the tear film post blink falls between the range of $2.3 \pm 1.5\mu\text{l}$, where most of the volume is located at the menisci [20].

Blinking occurs to re-wet the surface of the eye, via movement of the upper lid, and slight lower lid motion. Partial blinks are performed, where the upper lid only travels halfway down the the visible eye. Partial blinks tend to be performed during imaging when a person naturally blinks, instead of being instructed to do so [16]. The eye tends to remain open for between 5 and 10

seconds [11], where the tear film can flow tangentially along the surface of the eye, evaporate, or penetrate into the eye [16].

Experimentally, a collection of features of the tear film dynamics has been consistently observed when the eye is open. In what follows, we introduce some of these features to inform our modeling efforts. Tear film break-up occurs from thinning of the aqueous layer, likely caused by both tangential flows and evaporation. King-Smith [16] hypothesized that tangential flows influence the system in part by hastening the thinning rate of the tear film at the lid margins, referred to as the formation of the black line. Areas of increased lipid concentration, and lumps in the aqueous layer also contribute to occurrences of tangential flow, however evaporation is thought to dominate the thinning of larger areas of the tear film to cause tear film break-up [16]. King-Smith also determined that evaporation occurs across the healthy tear film, causing an average thinning rate of $\frac{11}{60}\mu\text{m/s}$ [16]. Using this rate, we can expect a $2.5\mu\text{m}$ thick tear film to thin completely in about 13.63 seconds. From the use of fluorescein in imaging the tear film, it has been observed that an upward drift of the lipid opposing gravity occurs proceeding the opening phase post-blink [16]. It has been hypothesized that the lipid layer causes surface tension gradients to produce a Marangoni flow, where less lipid and a higher surface tension is present near the upper lid compared to the lower lid. Upward drift of the lipid layer has been found to occur for approximately 2 seconds post-blink [16].

In this thesis, we create a model using a combination of continuum methods and constitutive equations, along with lubrication theory to represent the tear film. For the purpose of this study, we include the aqueous and lipid layers, and impose either specified lipid, mixed lipid, or no lipid flux boundary conditions for the open eye. For the blinking eye, we set the diffusive flux to zero. The system is solved numerically for cases of both the open and blinking eye.

II. LITERATURE REVIEW

Much work has been done to model the dynamics of the tear film during a blink and interblink (open eye). Braun's review [4] summarizes the collection of one-dimensional modeling efforts where the aqueous layer is considered a thin film of Newtonian fluid, and the lipid layer is modeled as an insoluble surfactant. In the one-dimensional models, the aqueous and lipid dynamics are approximated along a single line in the center of the eye running from the upper to the lower lids. Beginning with the single fluid aqueous models, the lipid layer is treated as a boundary as opposed to a separate layer. These models focus on capturing black line formation and tear

film breakup [21, 25, 28]. Results point towards the capillary pressure acting as the cause of black line formation at the menisci. Each model produces thinning at the black line reaching their set minimum tear film thickness near 10 seconds into the simulation, which is an arguably reasonable break up time for the tear film [4]. The lubrication models adequately approximate the shape of the aqueous layer near the black line when comparing to the numerical solution of the incompressible Navier-Stokes equations, and are used to maintain simplicity [29]. Effects of evaporation on the aqueous layer were also explored, causing more rapid thinning over a longer time span [5]. Results point towards evaporation being the main cause of large area tear film thinning and possible tear film break up, consistent with the hypothesis put forward by King-Smith [16].

Next, we discuss the findings considering the lipid layer as a concentration sitting on the surface of the aqueous layer [2, 10, 14]. The insoluble lipid acts as a surfactant, and undergoes advection from the interaction with the aqueous layer. All of the following works regard the aqueous layer as a thin film with the same material properties of water, where gravity influences evolution of the film. The influence of evaporation on the system was also included in the studies by [10, 14].

Jones et. al. [14] proposed a model for the vertical cross-section of the eye to study the aqueous and lipid layers; the goal of the work was to capture the experimentally observed upward drift of the tear film after the lids have been opened. Surface tension gradients caused by lipid concentration created surface flow, referred to as the Marangoni flow. At both lids, the tear film was pinned at 65 microns to be consistent with observation. Aqueous flux was not allowed at either lid as boundary conditions. For the lipid concentration, no diffusive flux was allowed at the boundaries. It was found that the evolution of the tear film can be significantly influenced by the lipid layer due to large surface tension gradients. In addition, it was found that the thickness profiles are sensitive to the initial lipid concentration. The model was able to produce upward drift of the lipid layer.

Aydemir et. al. [2] explored a similar model to Jones et. al., where different modeling choices included allowing aqueous flux at the boundaries and controlling the surface velocity at the lids. Flux was supplied through the space between the eye and the upper lid, and surface velocity was set to be equal to the lid speed. Numerical solutions required an initial tear film profile with a large volume to run for short times with a fine grid resolution. Increasing the lipid concentration caused a more apparent Marangoni effect, where a larger surface velocity drove lipid toward the upper lid. An overall thickening of the tear film was observed across the domain by increasing the lipid concentration. Similar to Aydemir, we are interested in capturing the upward drift of the lipid, as the lipid concentration is increased across the tear film.

Deng [10] considers the aqueous and lipid dynamics in a blinking rectangular domain, rather than the blinking one-dimensional line segment explored by Jones et. al. and Aydemir et. al. The lipid concentration was specified, and the tear film thickness was pinned at the boundaries. Aqueous flux was also specified at the lids. As a consequence, the surface velocity of the aqueous layer at the boundary was different from the lid speed. The surface velocity points towards the upper lid between blinks (the interblink period), signifying upward drift of the lipid layer. The solution for the tear film profile is similar to the findings of Aydemir et. al. and Jones et. al., where the volume of the tear film at the upper meniscus is much smaller compared to the volume at the lower meniscus by the end of the interblink period; however, draining of the aqueous layer from the upper lid occurs much more rapidly in Deng's model from the Marangoni effect. The slope of the lipid concentration must compensate for the specified value at the lids. As a result, more lipid is located at the lids during the interblink period, driving the Marangoni flow towards the center of the domain and draining the fluid at each lid. Similarly to Deng's work, we are interested in the presence of a lipid reservoir at each of the lids.

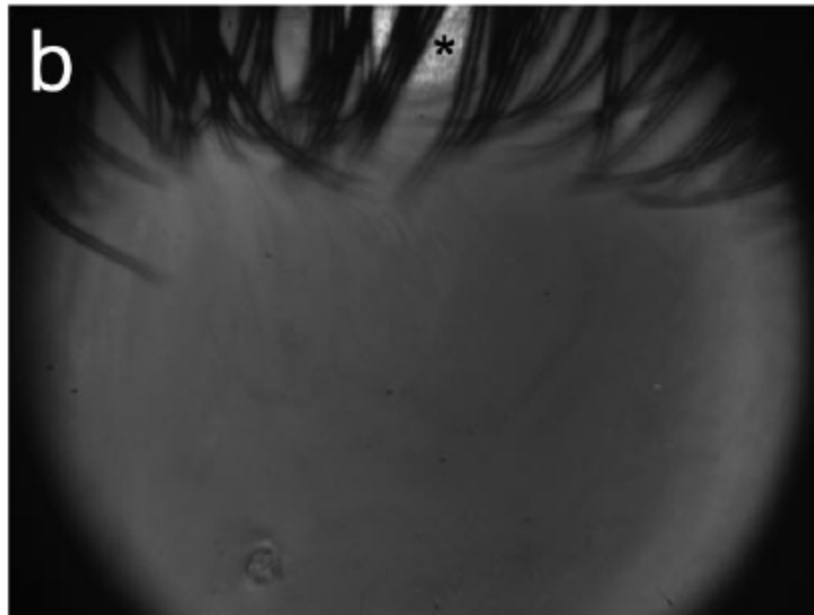


Figure 1: Picture capturing the possibility of the presence of a lipid reservoir near the upper lid. Lipid concentration is higher where the picture is more white. This picture was used with permission from Dr. King-Smith [15].

We are interested in capturing the tear film dynamics of a vertical cross section down the center of the eye, where a lipid reservoir is present and constantly supplying lipid to the system (see

Figure(1)). We impose the combination of a mixed or specified lipid boundary condition and controlling surface velocity at the lids. To our knowledge, this combination of boundary conditions has not been previously explored.

III. ONE DIMENSIONAL MODEL FOR THE TEAR FILM DYNAMICS

III.1 Model Formation

Aqueous Dynamics

For the purpose of this study, the healthy tear film will consist of an aqueous layer and a lipid layer [25]. Compared to the thickness of the tear film, the radius of the curvature of the eye is large, and so it is appropriate to assume that the surface of the eye is flat when modeling the tear film dynamics [2, 10, 14]. The fully open eye has a length of approximately 10mm. During a partial blink, the eye closes to about 5mm. If $H = 5\mu\text{m}$ is the typical thickness of the tear film, and $L_e = 5\text{mm}$ is the length of the half open eye from the bottom to the top lid, then $H \ll L_e$. It then follows that $\epsilon = \frac{H}{L_e} \ll 1$, and thus it is appropriate to assume the lubrication approximation [22].

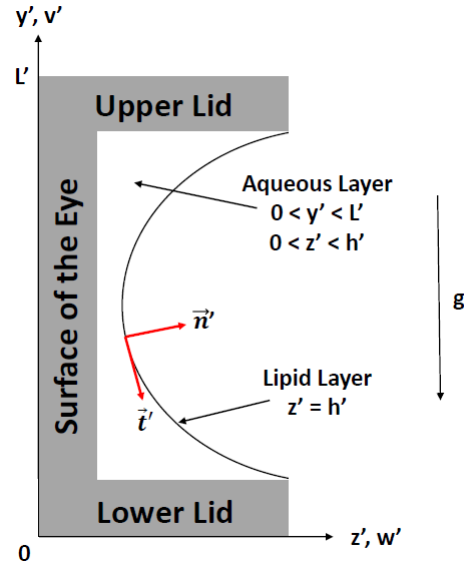


Figure 2: Schematic of the tear film for the mathematical model

Let $\vec{u}' = (v'(t', y', z'), w'(t', y', z'))$ represent the velocity field, where v' and w' are the velocities in the y' and z' directions respectively, and t' is the time. Also let p' denote the pressure inside of the

tear film. Note that all primed variables in this thesis represent dimensional values. Gravity, g , points in the negative y' direction. The coefficients ρ and μ represent the density and viscosity of the aqueous layer respectively.

To properly capture the behavior of the tear film, both momentum and mass must be conserved. Beginning with the body of the aqueous layer, we are interested in conserving the momentum in the y' and z' directions, expressed by the two dimensional Navier-Stokes equations

$$\rho \left(\frac{\partial \vec{u}'}{\partial t'} + (\vec{u}' \cdot \nabla') \vec{u}' \right) = -\nabla' p' + \mu (\nabla')^2 \vec{u}' + \rho g(-\hat{j}), \quad (\text{III.1})$$

where $\nabla' = \hat{e}_2 \frac{\partial}{\partial y'} + \hat{e}_3 \frac{\partial}{\partial z'}$ represents the gradient, $(\nabla')^2 = \nabla' \cdot \nabla'$ is the Laplace operator, and \hat{e}_2 along with \hat{e}_3 are unit vectors for the y' and z' directions respectively. The right hand side is composed of surface forces and body forces in total. Surface forces of a fluid include pressure forces and viscous forces. In our equation, the term $-\nabla' p'$ represents the pressure forces, and $\mu \nabla'^2 \vec{u}'$ represents the viscous force. The body force acting all over the tear film is gravity, expressed by $\rho g(-\hat{j})$. To complete the model, mass must be conserved:

$$\frac{\partial \rho}{\partial t'} + \nabla' \cdot (\rho \vec{u}') = 0.$$

The density does not change since the aqueous layer is assumed to be incompressible, and the term $\frac{\partial \rho}{\partial t'}$ is zero. The result is

$$\nabla' \cdot \vec{u}' = 0. \quad (\text{III.2})$$

Boundary Conditions at the Surface of the Eye

The mucus on the surface of the eye is wet by the aqueous tear film layer. Due to strong adhesive forces, the tear film spans across the surface of the eye. The fact that the tear film remains spread instead of clumping up demonstrates that the adhesive forces are stronger than the cohesive forces of the tear film. From this interaction, we know that fluid at the boundary must match the velocity of the stationary eye, which can be expressed by the no-slip condition specified by

$$v'(t', y', 0) = 0. \quad (\text{III.3})$$

In this model, it is assumed that the tear film is healthy. This implies that the salt concentration of the tear film is low, and thus no osmosis occurs between the eye and the tear film. We impose the

no-flux condition at the surface of the eye:

$$w'(t', y', 0) = 0. \quad (\text{III.4})$$

Boundary Conditions at the Aqueous-Lipid Interface

At any fluid-fluid interface, kinematic and dynamic conditions must be examined. In the case of the tear film, the interface between the lipid layer and the air forms a free surface. Beginning with the kinematic boundary condition, we incorporate the motion of the tear film at the interface by first letting $z' = h'(t', y')$ represent the tear film thickness. We define a vector \vec{r}' such that

$$\vec{r}'(t', y') = \hat{e}_2 y' + \hat{e}_3 h'(t', y'),$$

where the interfacial velocity of the tear film is represented by

$$\vec{v}'_I = \frac{\partial \vec{r}'}{\partial t'} = \hat{e}_3 \frac{\partial h'}{\partial t'}, \quad (\text{III.5})$$

and let the fluid velocity at the interface be represented by the velocity field

$$\vec{v}'_F = \hat{e}_2 v'(t', y', h') + \hat{e}_3 w'(t', y', h'). \quad (\text{III.6})$$

The evaporative mass flux of the tear film, E' , occurs directed normal to the boundary, removing fluid from the aqueous layer. Conserving mass, we express the fluid velocity at the interface as

$$(\vec{v}'_I - \vec{v}'_F) \cdot \vec{n}' = -\frac{E'}{\rho}, \quad (\text{III.7})$$

where the dot product including the unit normal, \vec{n}' , pointing from the tear film to the air, gives the velocity occurring at the aqueous-lipid interface induced by fluid motion. Using an equation of state for the evaporative mass flux derived by Ajaev [1], we determine the rate of evaporation from temperature and pressure differences (p'_0 is the reference air pressure, T' is the fluid temperature assumed constant at 310K, and T'_0 is the air temperature assumed constant at 300K), where

$$CE' = \alpha (p' - p'_0) + (T' - T'_0). \quad (\text{III.8})$$

When the tear film becomes thin, the pressure differences, due to the van der Waals force, can retard evaporation. The constant α is set to turn off evaporation at a specified tear film thickness.

From King-Smith, the average evaporation rate of the healthy tear film in an unsaturated, room temperature environment is measured to be $\frac{11}{60}\mu\text{m/s}$ [16]. This evaporation rate can be imposed by incorporating the value into the constant C .

To calculate the unit normal, we recall that $z' = h'(t', y')$ at the interface, and define

$$f' = z' - h'(t', y') = 0.$$

The unit normal pointing from the tear film to the air is then

$$\vec{n}' = \frac{\nabla' f'}{\|\nabla' f'\|} = \left(\hat{e}_2 \left(-\frac{\partial h'}{\partial y'} \right) + \hat{e}_3 \right) \left(\left(\frac{\partial h'}{\partial y'} \right)^2 + 1 \right)^{-1/2},$$

and since $\vec{t}' \cdot \vec{n}' = 0$, the unit tangent vector can be defined for later use as

$$\vec{t}' = \left(\hat{e}_2 + \hat{e}_3 \frac{\partial h'}{\partial y'} \right) \left(\left(\frac{\partial h'}{\partial y'} \right)^2 + 1 \right)^{-1/2}.$$

Returning to equation (III.7), we substitute the unit normal and the velocities into the kinematic boundary condition to find

$$-\frac{E'}{\rho} \left(\left(\frac{\partial h'}{\partial y'} \right)^2 + 1 \right)^{-1/2} = \frac{\partial h'}{\partial t'} + v'(t', y', h') \frac{\partial h'}{\partial y'} - w'(t', y', h'). \quad (\text{III.9})$$

For the dynamic boundary condition, stresses occurring in the normal and tangential directions must be balanced. Let $\mathbf{T}'^{(1)}$ be the stresses from the air, and let $\mathbf{T}'^{(2)}$ be stresses from the aqueous and lipid layers. Recalling that $z' = h'(t', y')$, we define the total stress tensor for the interface as $\mathbf{T}' = \mathbf{T}'^{(1)} - \mathbf{T}'^{(2)}$, where

$$\begin{aligned} \mathbf{T}'^{(1)} &= -p'_0 \mathbf{I}, \\ \mathbf{T}'^{(2)} &= -p' \mathbf{I} + \mu \left(\nabla' \vec{u}' + (\nabla' \vec{u}')^T \right), \end{aligned}$$

with \mathbf{I} being the two dimensional identity tensor. Influences of shear stress from the air on the tear film are assumed to be small. Both $\nabla' \vec{u}'$ and $(\nabla' \vec{u}')^T$ represent the Jacobian matrices of the surface velocity, with T representing the transpose. Performing the tensor product between \mathbf{T}' and \vec{n}' leads to an expression for the stress at the interface when $z' = h'(t', y')$. The term $\vec{n}' \cdot (\mathbf{T}' \cdot \vec{n}')$ will then incorporate the total stress occurring in the normal direction on the aqueous-lipid interface. Similarly for the tangential direction.

Continuing with the balancing of stress in the direction normal to the interface, we define γ' as surface tension. Multiplying the surface tension by the curvature of the interface, κ' , results in

the pressure at any point at the interface, known as the Young-Laplace equation. Simultaneously, the van der Waals force, Π' , points normal to the interface and holds the molecules together, maintaining the integrity of the tear film. The van der Waals force is responsible for the pressure caused by this interaction between the molecules. The total stress, F' , caused by the surface tension and the van der Waals force at the interface can then be expressed by:

$$F' = \gamma' \kappa' + \Pi'.$$

To balance normal stresses, our equation becomes

$$\vec{n}' \cdot (\mathbf{T}' \cdot \vec{n}') + F' = 0, \quad (\text{III.10})$$

We begin by solving the tensor product:

$$\begin{aligned} (\mathbf{T}' \cdot \vec{n}') &= \left(\hat{e}_2 \left(-\frac{\partial h'}{\partial y'} \left(-p'_0 + p' - 2\mu \frac{\partial v'}{\partial y'} \right) - \mu \left(\frac{\partial v'}{\partial z'} + \frac{\partial w'}{\partial y'} \right) \right) + \right. \\ &\left. \hat{e}_3 \left(\frac{\partial h'}{\partial y'} \mu \left(\frac{\partial w'}{\partial y'} + \frac{\partial v'}{\partial z'} \right) + \left(-p'_0 + p' - 2\mu \frac{\partial w'}{\partial z'} \right) \right) \right) \left(\left(\frac{\partial h'}{\partial y'} \right)^2 + 1 \right)^{-1/2}. \end{aligned}$$

Now the dot product to complete the first term of equation (III.10):

$$\vec{n}' \cdot (\mathbf{T}' \cdot \vec{n}') = (-p'_0 + p') + 2\mu \left(-\frac{\partial v'}{\partial y'} \left(\frac{\partial h'}{\partial y'} \right)^2 - \frac{\partial w'}{\partial z'} + \frac{\partial h'}{\partial y'} \left(\frac{\partial v'}{\partial z'} + \frac{\partial w'}{\partial y'} \right) \right) \left(\left(\frac{\partial h'}{\partial y'} \right)^2 + 1 \right)^{-1}. \quad (\text{III.11})$$

The second term of equation (III.10) just requires the calculation of the curvature, recalling again that $z' = h'(t', y')$:

$$\kappa'(h') = \frac{\partial^2 h'}{\partial y'^2} \left(\left(\frac{\partial h'}{\partial y'} \right)^2 + 1 \right)^{-3/2},$$

with the total stress expressed as

$$F' = \gamma' \left(\frac{\partial^2 h'}{\partial y'^2} \right) \left(1 + \left(\frac{\partial h'}{\partial y'} \right)^2 \right)^{-3/2} + \Pi', \quad (\text{III.12})$$

where $\Pi' = \frac{A}{h'^3}$ as used by [27], with A being the Hamaker constant. This equation shows that when the aqueous thickness becomes small, the pressure caused by the van der Waals force becomes low. When the surrounding pressures are large, the pressure gradients will cause aqueous flux towards the low pressure to maintain tear film integrity.

The tangential stress is calculated similarly to the normal stress, except instead of a dot product involving the unit normal, the unit tangent \vec{t}' is used, yielding $\vec{t}' \cdot (\mathbf{T}' \cdot \vec{n}')$. Motion caused by

the change in surface tension is known as the Marangoni effect. This is expressed by the dot product $\vec{t}' \cdot \nabla'_s \gamma'$, where ∇'_s represents the gradient with respect to the surface of the tear film. The balanced equation is then expressed as

$$\vec{t}' \cdot (\mathbf{T}' \cdot \vec{n}') + \vec{t}' \cdot \nabla'_s \gamma' = 0, \quad (\text{III.13})$$

and since we have already calculated $(\mathbf{T}' \cdot \vec{n}')$, we can skip to the first term in equation (III.13):

$$\vec{t}' \cdot (\mathbf{T}' \cdot \vec{n}') = \mu \left(2 \frac{\partial h'}{\partial y'} \frac{\partial v'}{\partial y'} - 2 \frac{\partial h'}{\partial y'} \frac{\partial w'}{\partial z'} + \left(\frac{\partial v'}{\partial z'} + \frac{\partial w'}{\partial y'} \right) \left(-1 + \left(\frac{\partial h'}{\partial y'} \right)^2 \right) \right) \left(\left(\frac{\partial h'}{\partial y'} \right)^2 + 1 \right)^{-1}. \quad (\text{III.14})$$

The second term of (III.13) is then calculated beginning with the surface gradient of the surface tension

$$\nabla'_s \gamma' = (\mathbf{I} - \vec{n}' \vec{n}') \cdot \nabla' \gamma' = \nabla' \gamma' - \vec{n}' (\vec{n}' \cdot \nabla' \gamma'),$$

and then the dot product with the tangential vector

$$\begin{aligned} -\vec{t}' \cdot \nabla'_s \gamma' &= -(\vec{t}' \cdot \nabla' \gamma' - (\vec{t}' \cdot \vec{n}') (\vec{n}' \cdot \nabla' \gamma')) = -\vec{t}' \cdot \nabla' \gamma' \\ &= -\frac{\partial \gamma'}{\partial y'} \left(\left(\frac{\partial h'}{\partial y'} \right)^2 + 1 \right)^{-1/2}. \end{aligned} \quad (\text{III.15})$$

Lipid Dynamics

To complete the model at the aqueous-lipid interface, the lipid layer must be modeled as well. The lipid layer is assumed to act as an insoluble surfactant on top of a moving tear film. A linear equation of state is used to express the relationship between surface tension and lipid concentration, expressed by as

$$\gamma' = \gamma_0 - RT\Gamma', \quad (\text{III.16})$$

where the term R is the universal gas constant, T is the tear film temperature, Γ' is the lipid concentration, and γ_0 is the initial surface tension of the tear film [8]. Γ' is expressed as an amount of lipid per area, which has the units of mol/m² in the case of the 2D tear film. To model this phenomena at the aqueous-lipid interface, we turn to an advective-surface diffusion equation for surfactant transport derived by Stone [26]:

$$\frac{\partial \Gamma'}{\partial t'} + \nabla'_s \cdot (\Gamma' \vec{u}'_s) + \Gamma' (\nabla'_s \cdot \vec{n}') (\vec{u}' \cdot \vec{n}') = D \nabla'^2_s \Gamma', \quad (\text{III.17})$$

where ∇'_s is the surface gradient

$$\nabla'_s = (\mathbf{I} - \vec{n}'\vec{n}') \cdot \nabla',$$

\vec{u}'_s is the velocity along the surface

$$\vec{u}'_s = (\mathbf{I} - \vec{n}'\vec{n}') \cdot \vec{u}',$$

and D is the coefficient representing the surface diffusion at the interface. The term $\nabla'_s \cdot (\Gamma' \vec{u}'_s)$ describes the advection at the interface, where lipid motion is determined by surface flows of the aqueous layer throughout the blink cycle. Redistribution of the lipid across new area of the tear film is determined by $\Gamma' (\nabla'_s \cdot \vec{n}') (\vec{u}' \cdot \vec{n}')$, which for the thin tear film, is arguably small. Surface diffusion occurs when there are changes in concentration gradients determined by $D \nabla_s'^2 \Gamma'$.

Boundary Conditions at the Lower and Upper Lids

In order to allow for a more natural evolution of the lipid layer near the lids, we introduce a mixed boundary condition controlling the amount of lipid at the boundary and the amount of lipid leaving the system. The lipid flux \vec{Q}'_Γ along the surface is expressed as

$$\vec{Q}'_\Gamma(t', y') = \Gamma' \vec{u}'_s - D \nabla_s' \Gamma'.$$

We then dot the tangential vector with the lipid flux vector to obtain

$$\begin{aligned} \vec{t}' \cdot \vec{Q}'_\Gamma(t', L') &= \vec{t}' \cdot (\Gamma' \vec{u}'_s) - \vec{t}' \cdot D \nabla_s' \Gamma' \Big|_{y'=L'}, \\ -\vec{t}' \cdot \vec{Q}'_\Gamma(t', 0) &= -\vec{t}' \cdot (\Gamma' \vec{u}'_s) + \vec{t}' \cdot D \nabla_s' \Gamma' \Big|_{y'=0}, \end{aligned}$$

where the positive or negative sign of the tangential vector directs the lipid flux out of the system through the upper or lower lid respectively.

The mixed boundary condition at each lid is given by:

$$\Gamma^* - \Gamma'(t', L') + B \left(\vec{t}' \cdot \vec{Q}'_\Gamma(t', L') \right) = 0, \quad \text{(III.18)}$$

$$\Gamma^* - \Gamma'(t', 0) + B \left(-\vec{t}' \cdot \vec{Q}'_\Gamma(t', 0) \right) = 0, \quad \text{(III.19)}$$

where the B of our choice has units s/m, and Γ^* is the dimensional lipid concentration we wish to specify at the boundary. The parameter B is used to weight the importance of the specified lipid

boundary condition versus the flux boundary condition. We discuss the parameter more in the next section.

The aqueous layer is pinned at the grey lines at both lids, which we express as

$$h'(t', 0) = h'(t', L') = h'_g. \quad (\text{III.20})$$

The surface velocities at the lids are assumed to be the same speed as the lid motion. We impose this by setting the surface velocity, u'_s , equal to the velocity of the lids to complete the boundary conditions:

$$\vec{u}'_s(t', L') = \hat{e}_2 \frac{dL'}{dt'}, \quad (\text{III.21})$$

$$\vec{u}'_s(t', 0) = \vec{0}, \quad (\text{III.22})$$

Initial Conditions

We assume the initial lipid concentration is uniform across the tear film, consistent with the boundary conditions at the dimensional value

$$\Gamma'(0, y') = \Gamma^*.$$

The initial tear film thickness is also expressed with a similar polynomial used by Deng [10]

$$h'(0, y') = h'_{typ} + (h'_g - h'_{typ}) \left(\frac{y'}{L_e} - 1 \right)^{2m},$$

where h'_{typ} is the typical tear film thickness at the center of the cross section of the eye, h'_g is the tear film thickness at the grey lines, and m determines the order of the polynomial. The initial volume can then be calculated by the following integral:

$$V'_i = \int_0^{L'} h'(0, y') dy'. \quad (\text{III.23})$$

III.2 Nondimensionalization

We use the following scales to nondimensionalize our model

$$y = \frac{y'}{L_e}, z = \frac{z'}{H}, h = \frac{h'}{H}, \epsilon = \frac{H}{L_e}, v = \frac{v'}{V}, w = \frac{w'}{\epsilon V}, t = \frac{t'}{L_e/V}, \Gamma = \frac{\Gamma'}{\Gamma^*},$$

$$p = (-p'_0 + p') \frac{H^2}{\mu V L_e}, T = \frac{T' - T'_0}{T_n}$$

where the description and numerical value of each scale is introduced in the table below:

Scaling		
Description:	Value:	Related Citation(s):
Typical tear film thickness	$H = 5 \times 10^{-6} \text{m}$	[4, 10, 16]
Half the distance between the eyelids	$L_e = 5 \times 10^{-3} \text{m}$	[4, 10]
Lipid concentration	$\Gamma^* = 4 \times 10^{-7} \text{mol/m}^2$	[2, 6, 10]
Average lid velocity	$V = 0.044 \text{m/s}$	[2, 28]
Viscosity of the aqueous layer	$\mu = 1.3 \times 10^{-3} \text{Ns/m}^2$	[2, 4, 10, 14]
Density of the aqueous layer	$\rho = 1.0 \times 10^3 \text{kg/m}^3$	[2, 4, 10, 14]
Initial surface tension	$\gamma_0 = 4.5 \times 10^{-2} \text{N/m}$	[2, 6, 10, 14]
Coefficient of surface diffusion	$D = 3 \times 10^{-8} \text{m}^2/\text{s}$	[2, 4, 10, 24]
Average rate of evaporation	$E = \frac{11}{60} \times 10^{-6} \text{m/s}$	[16]
Temperature scale	$T_n = 10 \text{K}$	

Aqueous Layer

Returning to the conservation of momentum (III.1), we begin with the momentum balance in the y -direction to obtain

$$\rho \left(\frac{\partial v'}{\partial t'} + v' \frac{\partial v'}{\partial y'} + w' \frac{\partial v'}{\partial z'} \right) = -\nabla p' + \mu \nabla^2 v' + \rho(-g).$$

After nondimensionalization, we find

$$\left(\frac{\rho V H \epsilon}{\mu} \right) \left(\frac{\partial v}{\partial t} + v \frac{\partial v}{\partial y} + w \frac{\partial v}{\partial z} \right) = -\frac{\partial p}{\partial y} + \left(\frac{\partial^2 v}{\partial y^2} (\epsilon^2) + \frac{\partial^2 v}{\partial z^2} \right) - \frac{\rho g H^2}{\mu V}.$$

The Reynolds number $Re = \frac{\rho V H}{\mu}$ is 0.169. A large Reynolds number amplifies the acceleration of the fluid to cause turbulent flows, where a smaller Reynolds number diminishes the effect of the changes in velocity resulting in a laminar flow. We are interested in examining the leading order equations representing the tear film. Thus, any term with an order smaller than $O(\epsilon)$ is regarded as negligible. Since $Re < 1$, we argue that the Reynolds number has a negligible effect on the tear film regarding the y -direction. After removing small terms and letting $G = \frac{\rho g H^2}{\mu V}$, we

are left with

$$-\frac{\partial p}{\partial y} + \frac{\partial^2 v}{\partial z^2} - G = 0.$$

Moving on to the conservation of momentum (III.1) in the z -direction, we recall that

$$\rho \left(\frac{\partial w'}{\partial t'} + v' \frac{\partial w'}{\partial y'} + w' \frac{\partial w'}{\partial z'} \right) = -\nabla p' + \mu \nabla^2 w'.$$

Again, nondimensionalized parameters are substituted into the equation:

$$\left(\frac{\rho V H \epsilon^3}{\mu} \right) \left(\frac{\partial w}{\partial t} + v \frac{\partial w}{\partial y} + w \frac{\partial w}{\partial z} \right) = -\frac{\partial p}{\partial z} + \left(\frac{\partial^2 w}{\partial y^2} (\epsilon^4) + \frac{\partial^2 w}{\partial z^2} (\epsilon^2) \right).$$

The Reynolds number is again small, where $(Re) \epsilon^3 \ll \epsilon$. Removing all higher order ϵ terms, we obtain

$$\frac{\partial p}{\partial z} = 0.$$

The nondimensional conservation of mass (III.2) is

$$\frac{\partial v}{\partial y} + \frac{\partial w}{\partial z} = 0.$$

Boundary Conditions at the Aqueous-Lipid Interface

For the kinematic boundary condition (III.9), we again apply our nondimensionalization to find

$$-E^* (p\alpha^* + T) = \frac{\partial h}{\partial t} + v \frac{\partial h}{\partial y} - w,$$

where $E^* = \frac{1}{CV\epsilon\rho}$, and $\alpha^* = \frac{VL_e\alpha\mu}{H^2}$.

We continue the nondimensionalization of the dynamic boundary condition in the normal direction (equations (III.11) and (III.12)). Here, we assume that

$$\gamma \approx \gamma_0,$$

which can be argued with the scaling, where the term containing Γ decreases the surface tension by ϵ . After nondimensionalization, we let $S = \frac{\gamma_0\epsilon^3}{\mu V}$ and $A^* = \frac{\epsilon A}{\mu V H^2}$ to obtain

$$p = -S \frac{\partial^2 h}{\partial y^2} - \frac{A^*}{h^3}.$$

Again, we apply the nondimensionalization to the dynamic boundary condition in the tangential direction (equations (III.14) and (III.15)), remove terms containing higher order ϵ , and let $Ma = \frac{RT\Gamma_0}{\mu V}$ to obtain

$$\frac{\partial v}{\partial z} = -\epsilon Ma \frac{\partial \Gamma}{\partial y}.$$

In order to understand the influence of surface tension on the tear film dynamics, we retain the capillarity term S and the Marangoni term Ma .

Finally, we nondimensionalize the equation for the evolution of the lipid concentration (III.17)

$$\frac{\partial \Gamma}{\partial t} + \frac{\partial}{\partial y} (\Gamma v_s) - \frac{D}{VL_e} \frac{\partial^2 \Gamma}{\partial y^2} = 0,$$

where $Pe = \frac{VL_e}{D} = 7.3333 \times 10^3$ is the Peclet number, $\frac{1}{Pe} = 1.3636 \times 10^{-4}$ from the above table, and $v_s = v(t, y, h)$. Although arguably small, we choose to keep the diffusive term in our system, in contrast to Aydemir et. al.

Boundary Conditions at the lids

The mixed boundary conditions, when nondimensionalized, become

$$(1 - \Gamma(t, L)) + B^* \left(\frac{dL}{dt} \Gamma(t, L) - \frac{1}{Pe} \frac{\partial \Gamma}{\partial y}(t, L) \right) = 0 \quad \text{(III.24)}$$

$$(1 - \Gamma(t, 0)) + B^* \left(\frac{1}{Pe} \frac{\partial \Gamma}{\partial y}(t, 0) \right) = 0 \quad \text{(III.25)}$$

where $B^* = \frac{BD}{L_e}$.

The mixed boundary condition can be manipulated to explore specified lipid, and no lipid flux conditions as well. Specifically, when $B^* = 0$ we are left with a specified lipid at the upper and lower lid boundaries, where

$$\Gamma(t, L) = 1,$$

$$\Gamma(t, 0) = 1,$$

and as B^* grows large, the mixed boundary condition at the upper lid is expressed by

$$0 = \lim_{B^* \rightarrow \infty} \left(\frac{1 - \Gamma(t, L)}{B^*} + \frac{dL}{dt} \Gamma(t, L) - \frac{1}{Pe} \frac{\partial \Gamma}{\partial y}(t, L) \right) = \frac{dL}{dt} \Gamma(t, L) - \frac{1}{Pe} \frac{\partial \Gamma}{\partial y}(t, L),$$

and at the lower lid,

$$0 = \lim_{B^* \rightarrow \infty} \left(\frac{1 - \Gamma(t, 0)}{B^*} + \left(\frac{1}{Pe} \frac{\partial \Gamma}{\partial y}(t, 0) \right) \right) = \left(\frac{1}{Pe} \frac{\partial \Gamma}{\partial y}(t, 0) \right),$$

to produce a no lipid flux boundary condition.

III.3 Governing Equations for the Tear Film Dynamics

To summarize, the leading-order equations determining the aqueous dynamics are:

$$-\frac{\partial p}{\partial y} + \frac{\partial^2 v}{\partial z^2} - G = 0, \quad (\text{III.26})$$

$$\frac{\partial p}{\partial z} = 0, \quad (\text{III.27})$$

$$\frac{\partial v}{\partial y} + \frac{\partial w}{\partial z} = 0. \quad (\text{III.28})$$

At $z = 0$, we have:

$$v = 0, \quad (\text{III.29})$$

$$w = 0. \quad (\text{III.30})$$

At $z = h$, the leading order boundary conditions are:

$$\frac{\partial v}{\partial z} = -\epsilon Ma \frac{\partial \Gamma}{\partial y}, \quad (\text{III.31})$$

$$-E^* (p\alpha^* + T) = \frac{\partial h}{\partial t} + v \frac{\partial h}{\partial y} - w, \quad (\text{III.32})$$

$$p = -S \frac{\partial^2 h}{\partial y^2} - \frac{A^*}{h^3}. \quad (\text{III.33})$$

Finally, the lipid dynamics are governed by surface velocity and surface diffusion:

$$\frac{\partial \Gamma}{\partial t} + \frac{\partial}{\partial y} (\Gamma v_s) - \frac{1}{Pe} \frac{\partial^2 \Gamma}{\partial y^2} = 0. \quad (\text{III.34})$$

To form the thin film equation, we return to the nondimensionalized kinematic boundary condition.

Recalling equation (III.28), we can integrate to find

$$-w(t, y, h) = \int_0^h \frac{\partial v}{\partial y} dz,$$

which we substitute into equation (III.32), to obtain

$$-E(p\alpha^* + T) = \frac{\partial h}{\partial t} + v(t, y, h) \frac{\partial h}{\partial y} + \int_0^h \frac{\partial v}{\partial y} dz. \quad (\text{III.35})$$

By the Liebniz Rule, we know that

$$\frac{\partial}{\partial y} \left(\int_0^h v dz \right) = \int_0^h \frac{\partial v}{\partial y} dz + v(t, y, h) \frac{\partial h}{\partial y},$$

and we substitute into equation (III.35) to find

$$-E(p\alpha^* + T) = \frac{\partial h}{\partial t} + \frac{\partial}{\partial y} \left(\int_0^h v dz \right). \quad (\text{III.36})$$

To find v , the nondimensional simplified momentum equation is solved, starting with equation (III.26)

$$\frac{\partial^2 v}{\partial z^2} = \frac{\partial p}{\partial y} + G.$$

With the boundary condition found from the tangential stress (III.31), we obtain

$$\frac{\partial v}{\partial z} = \left(\frac{\partial p}{\partial y} + G \right) z - \left(\frac{\partial p}{\partial y} + G \right) h - \epsilon Ma \frac{\partial \Gamma}{\partial y}.$$

The boundary condition from the no-slip condition (III.29) is then used, finding v to be

$$v = \left(\frac{\partial p}{\partial y} + G \right) \left(\frac{z}{2} - h \right) z - \epsilon Ma \frac{\partial \Gamma}{\partial y} z. \quad (\text{III.37})$$

Let $Q = \int_0^h v dz$ be the flux, where

$$Q = -\frac{h^3}{3} \left(\frac{\partial p}{\partial y} + G \right) - \epsilon Ma \frac{\partial \Gamma}{\partial y} \frac{h^2}{2}, \quad (\text{III.38})$$

which we substitute into equation (III.36) to obtain

$$\frac{\partial h}{\partial t} = -\frac{\partial}{\partial y} \left(-\frac{h^3}{3} \left(\frac{\partial p}{\partial y} + G \right) - \epsilon Ma \frac{\partial \Gamma}{\partial y} \frac{h^2}{2} \right) - E^* (p\alpha^* + T). \quad (\text{III.39})$$

Thus, we must solve the coupled system of nonlinear partial differential equations,

$$\frac{\partial h}{\partial t} = -\frac{\partial}{\partial y} \left(-\frac{h^3}{3} \left(\frac{\partial p}{\partial y} + G \right) - \epsilon Ma \frac{\partial \Gamma}{\partial y} \frac{h^2}{2} \right) - E^* (p\alpha^* + T), \quad (\text{III.40})$$

$$p(t, y) = -S \frac{\partial^2 h}{\partial y^2} - \frac{A^*}{h^3}, \quad (\text{III.41})$$

$$\frac{\partial \Gamma}{\partial t} + \frac{\partial}{\partial y} (\Gamma v_s) - \frac{1}{Pe} \frac{\partial^2 \Gamma}{\partial y^2} = 0, \quad (\text{III.42})$$

where $v_s(t, y)$, for $h(t, y)$, $p(t, y)$, and $\Gamma(t, y)$ on the domain $0 < y < L$. Boundary conditions at the upper lid, $y = L$, and lower lid, $y = 0$, are given by:

$$h(t, L) = \frac{h_g}{H},$$

$$\begin{aligned}
v_s(t, L) &= \frac{dL}{dt}, \\
h(t, 0) &= \frac{h_g}{H}, \\
v_s(t, 0) &= 0,
\end{aligned}$$

with the mixed boundary conditions for the lipid,

$$(1 - \Gamma(t, L)) + B^* \left(\frac{dL}{dt} \Gamma(t, L) - \frac{1}{Pe} \frac{\partial \Gamma}{\partial y}(t, L) \right) = 0, \quad (\text{III.43})$$

$$(1 - \Gamma(t, 0)) + B^* \left(\frac{1}{Pe} \frac{\partial \Gamma}{\partial y}(t, 0) \right) = 0. \quad (\text{III.44})$$

The nondimensionalized initial conditions are given by

$$h(0, y) = \frac{h_{typ} + (h_g - h_{typ})(y - 1)^{2m}}{H}, \quad (\text{III.45})$$

$$\Gamma(0, y) = 1. \quad (\text{III.46})$$

IV. NUMERICAL METHOD

To compute the blink, we used a similar strategy as Maki [19] by mapping our moving domain to a fixed domain through the use of a change of variables, influenced by the Overture framework created by Henshaw [9]. However, here we do not include overlapping grids. Instead we use only the background grid to compute the solution of the moving system. Beginning with the parameterization, we let $0 \leq s \leq 1$ represent the fixed domain, and y represent the real domain, such that:

$$\begin{aligned}
G(t, y) &= s = \frac{y}{L(t)}, \\
G^{-1}(t, s) &= y = sL(t).
\end{aligned}$$

Now we calculate the derivatives with respect to time and space on the fixed domain by letting \hat{h} denote the tear film thickness:

$$\hat{h}(t, s) = h(t, G^{-1}(t, s)).$$

First we find the derivative of the tear film thickness with respect to time by the chain rule:

$$\frac{\partial h}{\partial t} = \frac{\partial \hat{h}}{\partial t} + \frac{\partial \hat{h}}{\partial s} \frac{\partial s}{\partial t}, \quad (\text{IV.1})$$

where the derivative of s with respect to time is expressed by

$$\frac{\partial s}{\partial t} = \frac{\partial}{\partial t} (G(t, y)) = \frac{\partial}{\partial t} \left(\frac{y}{L(t)} \right) = \left(-\frac{dL(t)}{dt} \right) \left(\frac{y}{L(t)^2} \right) = \left(-\frac{dL(t)}{dt} \right) \left(\frac{s}{L(t)} \right),$$

which we substitute into equation (IV.1), obtaining

$$\frac{\partial h}{\partial t} = \frac{\partial \hat{h}}{\partial t} + \frac{\partial \hat{h}}{\partial s} \left(-\frac{dL(t)}{dt} \right) \left(\frac{s}{L(t)} \right).$$

Now derivatives with respect to space for the tear film thickness again using the chain rule:

$$\frac{\partial h}{\partial y} = \frac{\partial \hat{h}}{\partial s} \frac{\partial s}{\partial y}, \quad (\text{IV.2})$$

where the derivative of s with respect to y is

$$\frac{\partial s}{\partial y} = \frac{\partial}{\partial y} \left(\frac{y}{L(t)} \right) = \left(\frac{1}{L(t)} \right),$$

which we substitute into equation (IV.2) to give

$$\frac{\partial h}{\partial y} = \frac{\partial \hat{h}}{\partial s} \left(\frac{1}{L(t)} \right).$$

For the second derivative,

$$\frac{\partial^2 h}{\partial y^2} = \frac{\partial^2 \hat{h}}{\partial s^2} \left(\frac{\partial s}{\partial y} \right)^2 + \frac{\partial \hat{h}}{\partial s} \frac{\partial^2 s}{\partial y^2},$$

and we substitute the previously found derivative of s with respect to y to obtain

$$\frac{\partial^2 h}{\partial y^2} = \frac{\partial^2 \hat{h}}{\partial s^2} \left(\frac{1}{L(t)} \right)^2.$$

Substitution into the tear film equation yields

$$\begin{aligned} \frac{\partial \hat{h}}{\partial t} = & \frac{\partial \hat{h}}{\partial s} \left(\frac{\hat{h}^2}{L(t)} \right) \left(\frac{\partial \hat{p}}{\partial s} \left(\frac{1}{L(t)} \right) + G \right) + \frac{\partial^2 \hat{p}}{\partial s^2} \left(\frac{\hat{h}^3}{3L(t)^2} \right) + \epsilon Ma \frac{\partial^2 \hat{\Gamma}}{\partial s^2} \left(\frac{\hat{h}^2}{2L(t)^2} \right) + \\ & \epsilon Ma \left(\frac{\partial \hat{\Gamma}}{\partial s} \frac{\partial \hat{h}}{\partial s} \right) \left(\frac{\hat{h}}{L(t)^2} \right) - E^* (\hat{p}\alpha^* + T) + \left(\frac{\partial \hat{h}}{\partial s} \frac{dL}{dt} \right) \left(\frac{s}{L(t)} \right). \end{aligned} \quad (\text{IV.3})$$

The pressure is similarly mapped to the fixed domain to give

$$\hat{p} = -S \frac{\partial^2 \hat{h}}{\partial s^2} \left(\frac{1}{L(t)^2} \right) - \frac{A^*}{h^3} \quad (\text{IV.4})$$

Lastly, we map the lipid concentration evolution onto the fixed domain to obtain

$$\frac{\partial \hat{\Gamma}}{\partial t} = \frac{\partial \hat{\Gamma}}{\partial s} \left(\frac{\hat{h}^2}{2L(t)} \right) \left(\frac{\partial \hat{p}}{\partial s} \left(\frac{1}{L(t)} \right) + G \right) + \epsilon Ma \left(\frac{\partial \hat{\Gamma}}{\partial s} \right)^2 \frac{\hat{h}}{L(t)^2} + \hat{\Gamma} \left(\frac{\partial^2 \hat{p}}{\partial s^2} \right) \left(\frac{\hat{h}^2}{2L(t)^2} \right) +$$

$$\begin{aligned} \hat{\Gamma} \left(\frac{\partial \hat{p}}{\partial s} \left(\frac{1}{L(t)} \right) + G \right) \left(\frac{\partial \hat{h}}{\partial s} \frac{\hat{h}}{L(t)} \right) + \hat{\Gamma} \epsilon Ma \left(\frac{\partial^2 \hat{\Gamma}}{\partial s^2} \frac{\hat{h}}{L(t)^2} \right) + \hat{\Gamma} \epsilon Ma \left(\frac{\partial \hat{\Gamma}}{\partial s} \frac{\partial \hat{h}}{\partial s} \frac{1}{L(t)^2} \right) + \\ \frac{1}{Pe} \left(\frac{\partial^2 \hat{\Gamma}}{\partial s^2} \frac{1}{L(t)^2} \right) + \left(\frac{\partial \hat{\Gamma}}{\partial s} \frac{dL}{dt} \right) \left(\frac{s}{L(t)} \right). \end{aligned} \quad (IV.5)$$

A method of lines was implemented to solve the mapped system. We approximated all spatial derivatives with second order finite differences, and used the ode15s solver within MATLAB to integrate the remaining system of ordinary differential equations forward in time.

To validate our numerical scheme, we checked whether the volume of the tear film was conserved, which was computed by integrating the evolution equation:

$$\int_0^{L(t)} \frac{\partial h}{\partial t} dy = \int_0^{L(t)} \left(-\frac{\partial Q}{\partial y} - E(\alpha^* + T) \right) dy,$$

which can be solved through the use of Leibniz's rule

$$\begin{aligned} V(t) - V(0) &= \int_0^t \left(h(t, L(t)) \frac{dL(t)}{dt} - Q(t, L(t)) + Q(t, 0) - \int_0^{L(t)} E^*(p(t, y) \alpha^* + T) dy \right) dt. \\ \frac{dV}{dt} &= h(t, L(t)) \frac{dL}{dt} - Q(t, L(t)) + Q(t, 0) - \int_0^{L(t)} E^*(p \alpha^* + T) dy \end{aligned} \quad (IV.6)$$

The conservation of volume is evidenced by the following graphs, where we check if volume is conserved properly for the mixed boundary conditions when the eye is open.

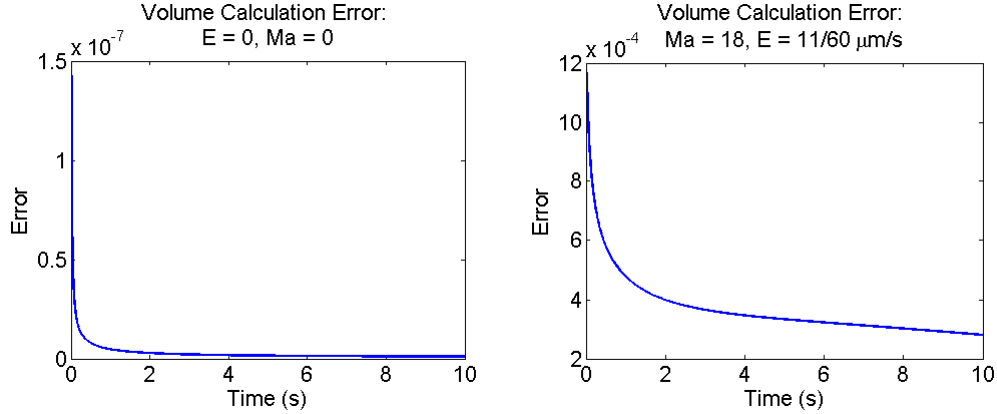


Figure 3: On the left is the error for the volume calculation in the case where evaporation and the Marangoni effect are turned off. On the right, the figure displays the volume calculation error when evaporation and the Marangoni effect are activated.

The approximate volume of the system was calculated using the trapz function within MATLAB on the approximation of the tear film thickness, $h(t, y)$, found from the numerical method. Error

was found by subtracting the approximate volume from the volume found by solving equation (IV.6). When $Ma = 0$ and $E = 0$, volume is conserved, as $\frac{dV}{dt} = 0$. Otherwise, when $Ma \neq 0$ and $E \neq 0$, $\frac{dV}{dt}$ was approximated using Euler's method.

With evaporation and the Marangoni effect turned off, volume is successfully conserved within the system, evidenced by the corresponding converging error plot. Evaporation will decrease the amount of fluid in the system, and having the Marangoni effect on allows flux in and out of the system. The error converges with these effects, however to keep the surface velocity smooth, a high grid resolution needed to be maintained (e.g. 16383 grid points were used for the fixed domain).

V. NUMERICAL SOLUTION - OPEN EYE

We begin our analysis with the open eye post blink, for an interblink period of 6.8 seconds when the Marangoni effect is turned off. The thickness of the tear film at the grey line is set to reach $h'_g = 65\mu\text{m}$. At the center of the domain, the typical tear film thickness was set to be $h'_{typ} = 2.5\mu\text{m}$. The simulations presented throughout the thesis were run with a typical tear film thickness at both $5\mu\text{m}$, and $2.5\mu\text{m}$. It was found that the relationships between thickness, lipid concentration, and pressure did not change between these two thicknesses. We also observed that the code was not able to integrate forward in time beyond 1 nondimensional second in the simulation with the larger thickness due to the increased positive flux at the upper lid, causing more rapid draining near the black line.

The order of the initial condition polynomial is $m = 10$ for the tear film thickness (III.45). From the nondimensional area, we multiplied by $5\mu\text{m}$ for the tear film thickness, and $10000\mu\text{m}$ (1cm) for the vertical cross section of the eye. In order to convert to a volume (μl), we multiply by the long dimension of the palpebral fissure at an approximate length of $25000\mu\text{m}$ (2.5cm). The total approximate dimensional initial volume of the system was then calculated to be $1.369\mu\text{l}$. It is important to mention that by using $2.5\mu\text{m}$ as the typical thickness and $m = 10$, there is less volume initially present in the tear film than observed experimentally [20]. We found that decreasing the order of polynomial resulted in a larger curvature of the tear film near the menisci, influencing the pressure and therefore flux at the lids while increasing the initial volume of the tear film (III.23). As a consequence of the larger positive fluxes at the lids, we couldn't integrate forward for long times. A uniform lipid concentration profile was enforced at the nondimensional value across the tear film, again maintaining consistency with the boundary conditions.

In what follows, we present an exploration of the influence of a lipid boundary condition on the tear film dynamics by varying the parameter B^* in the boundary condition equations (III.43) and (III.44) to determine lipid flux. To begin, in Section V.1, we set $B^* = 0$, and study the influence of a lipid reservoir at the upper and lower lids. In Section V.2, we analyze the influence of nonzero values of B^* on the tear film dynamics. To our knowledge, the mixed lipid boundary condition has not been previously studied.

V.1 Study of the Tear Film Dynamics with a Lipid Reservoir at the Lids

V.1.1 Marangoni Effect Turned Off

To begin, we set the Marangoni number equal to zero to decouple the aqueous and lipid dynamics given by equations (III.40) and (III.42). This simplification turns off the Marangoni effect and allows the influence of gravity and evaporation to be explored. In the following plots, the time spacing between each curve is 1.136s.

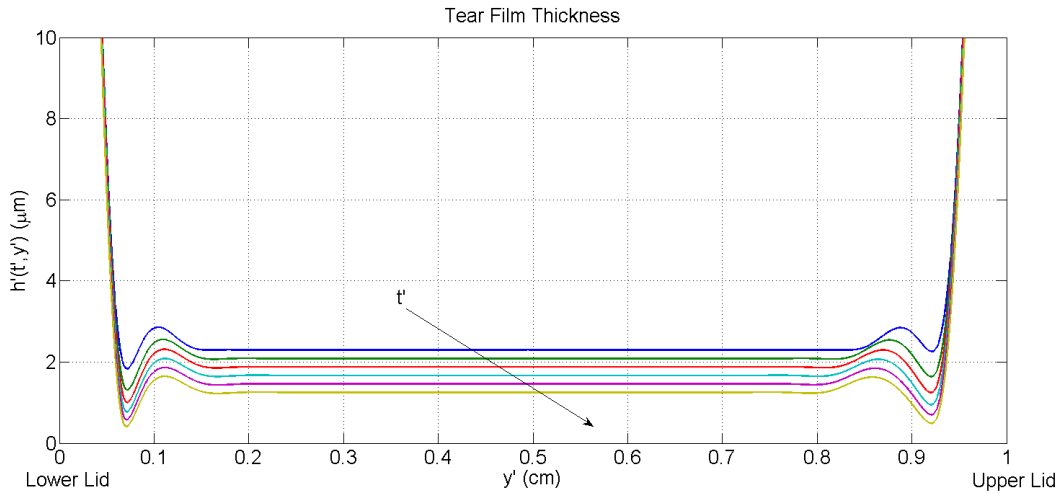


Figure 4: Aqueous layer evolution between $t = 1.14$ s and $t = 6.82$ s from equation (III.40).

Figure (4) shows the evolution of the profile of the tear film when the eye remains open for 6.82 seconds. For future reference, the surface of the eye is located at $z' = 0$ microns, the lower lid at $y' = 0$ cm, and the upper lid at $y' = 1$ cm. Most tear fluid is located within the menisci near the lids, where pressure gradients induced by surface tension cause fluid motion directed towards the lids. The positive curvature of the tear film at the menisci generates a low pressure in comparison to the flat film between the menisci, referred to as meniscus-induced-thinning [3]. As a result, black

lines form near the menisci, where the tear film reaches its minimum thickness, and continues to thin throughout the simulation. Next to the menisci, the tear film thickness increases slightly as a capillary ridge forms due to the surface-tension-induced redistribution of fluid, as observed in previous studies [4]. Gravity drives fluid towards the lower lid across the domain, and evaporation continually thins the tear film. Both of these effects are most apparent in the evolution of the tear film thickness at the center of the domain.

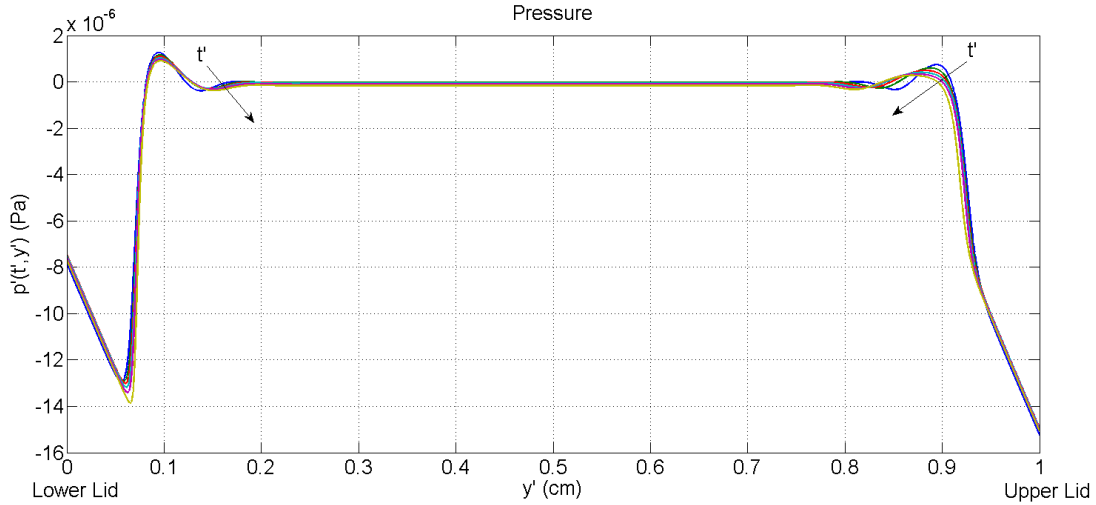


Figure 5: Pressure of the system between $t' = 1.14\text{s}$ and $t' = 6.82\text{s}$ from equation (III.41).

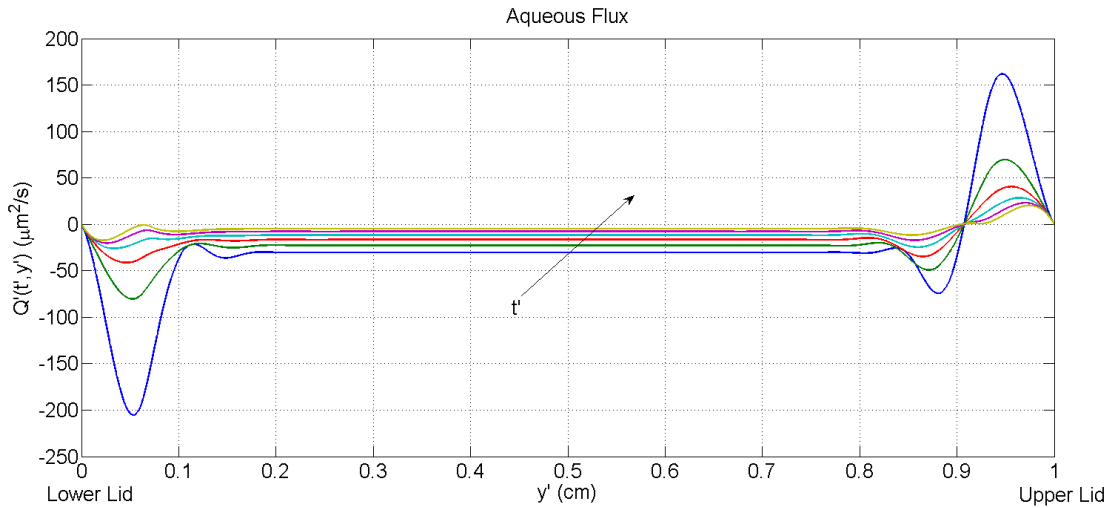


Figure 6: Aqueous flux between $t' = 1.14\text{s}$ and $t' = 6.82\text{s}$ from equation (III.38).

The evolution of the pressure is shown in Figure (5). Pressure profiles do not change drastically, as the curvature of the tear film (surface tension effect) and its thickness (van der Waals effect) do

not greatly differ with time. In the lower pressure regions in the menisci, the pressure gradient is evolving to the value $-G$. As a consequence, the flux, given by

$$Q = -\frac{h^3}{3} \left(\frac{\partial p}{\partial y} + G \right),$$

as shown in Figure (6), seems to tend towards zero as the simulation goes on. In the upper meniscus, the positive flux indicates that capillarity-induced thinning dominates over the effect of gravity. In the lower meniscus, the effect of gravity and capillarity-induced thinning work together pump fluid into the lower meniscus. The flux is small but negative between the menisci due to gravity.

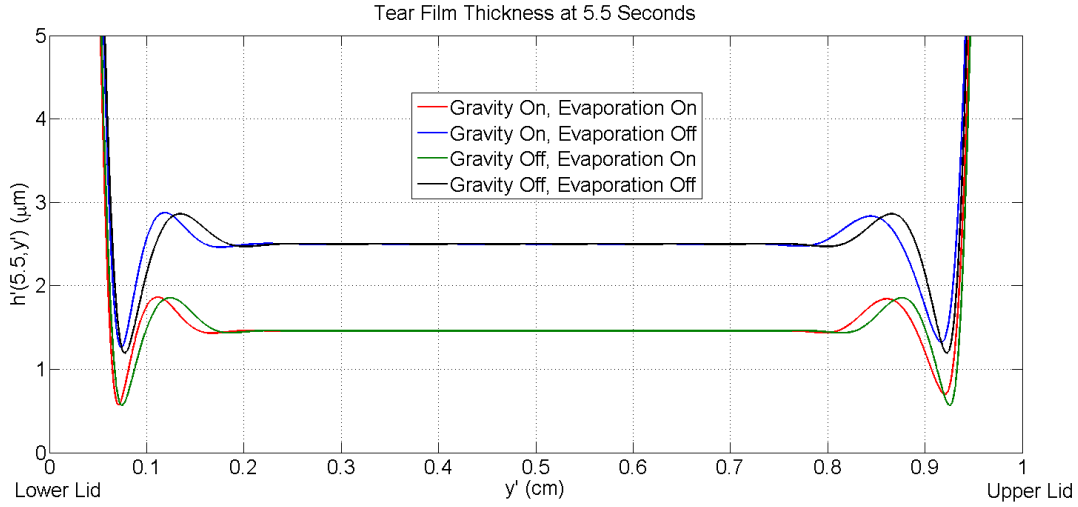


Figure 7: Influence of gravity and evaporation on the tear film at $t' = 5.5s$ from equation (III.40).

The overall influence of gravity and evaporation on the aqueous dynamics is best summarized in Figure (7), where the tear film thickness is shown at 5.5 seconds. With evaporation turned on, the entire tear film thins. In the center of the domain, the tear film thickness decreases by approximately 1 micron ($\frac{11}{60} \mu\text{m/s} \times 5.5s$). Gravity breaks the symmetry of the tear film profile with the minimum tear film thickness still occurring in the black line region, but now at the lower lid. In addition, gravity shifts the tear film profile towards the lower lid.

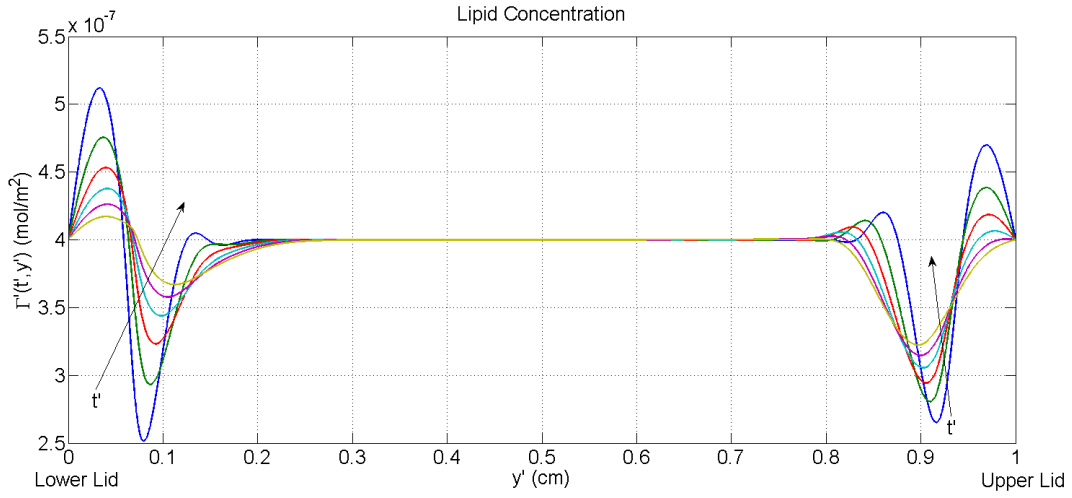


Figure 8: Evolution of the polar lipid concentration between $t' = 1.14s$ and $t' = 6.82s$ from equation (III.42).

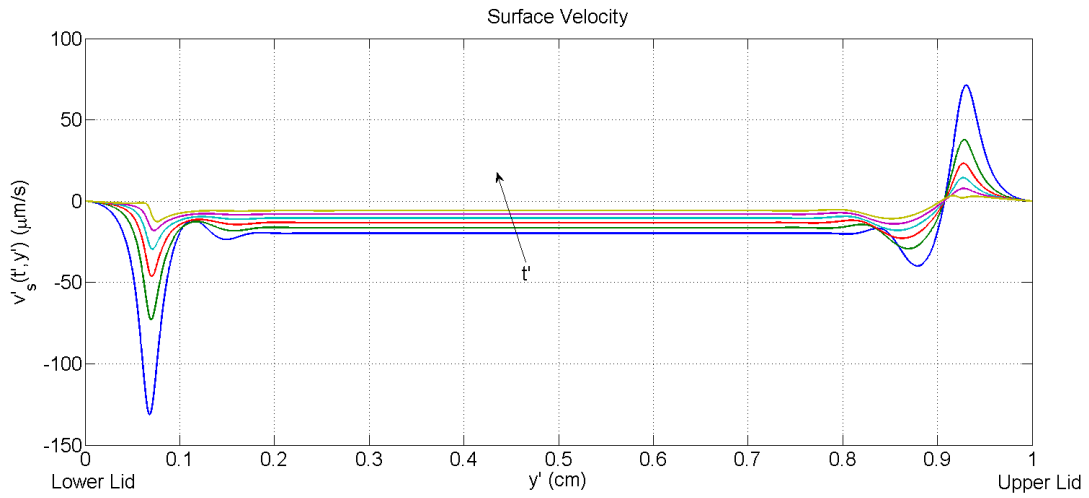


Figure 9: Surface velocity between $t' = 1.14s$ and $t' = 6.82s$ from equation (III.37).

The lipid dynamics, shown in Figure (8), is determined by both the surface velocity and surface diffusion. Surface velocity, Figure (9), advects the lipid towards the lower lid, except in the upper meniscus where the surface velocity is dominated by the capillarity-induced thinning to pull the lipid into the upper meniscus. As the lipid begins to collect in the menisci, surface diffusion smooths out the gradients in the lipid. The lipid dynamics do not significantly change at the center of the domain when the Marangoni effect is turned off.

V.1.2 Marangoni Effect Turned On

With the Marangoni number on, the equations determining the evolution of the aqueous and lipid layers are now coupled, (III.40) and (III.42). In the simulations that follow, the influence of evaporation and gravity remain on, and will have the same influence on the system as discussed in the previous subsection. Recall that $B^* = 0$ produces results in the presence of a lipid reservoir at both lids. The following results show the evolution on the open eye system between 1.14s and 9.09s, again with a time spacing of 1.136s between each curve.

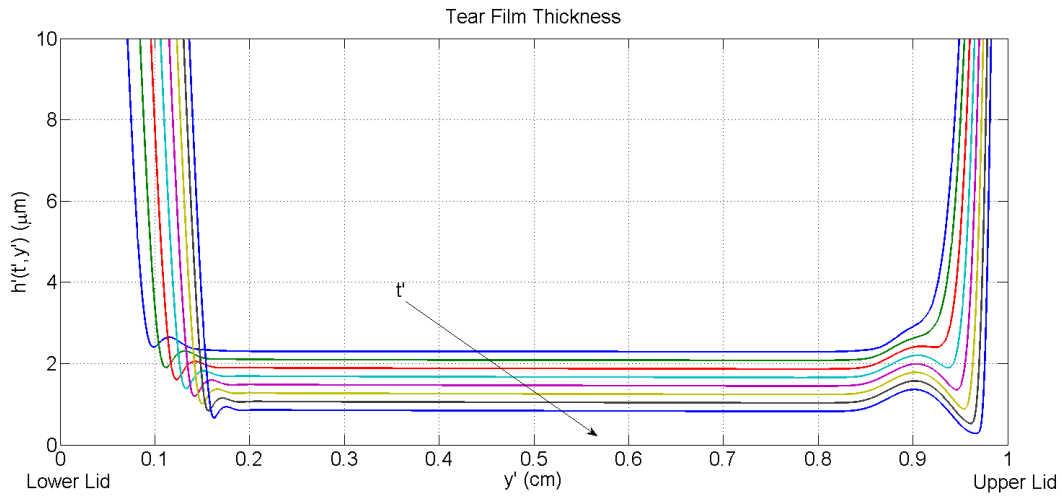


Figure 10: Aqueous layer between $t' = 1.14\text{s}$ and $t' = 9.09\text{s}$ from equation (III.40).

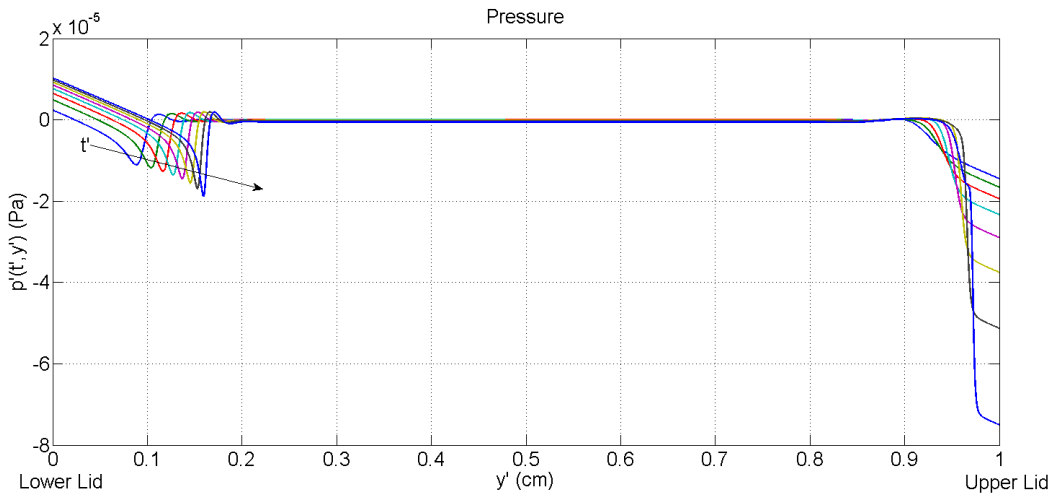


Figure 11: Pressure of the system between $t' = 1.14\text{s}$ and $t' = 9.09\text{s}$ from equation (III.41).

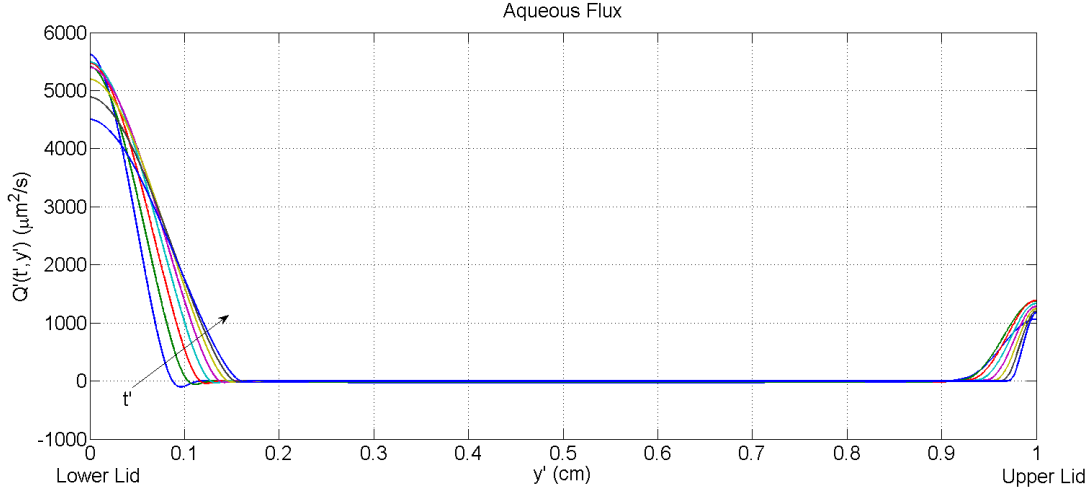


Figure 12: Aqueous flux between $t' = 1.14\text{s}$ and $t' = 9.09\text{s}$ from equation (III.38).

Figure (10) shows the evolution of the tear film profile when the Marangoni effect is turned on. As before, the tear film continuously thins at the center of the domain. Now, more fluid is present in the lower meniscus compared to the upper meniscus. A black line still forms at the edge of the upper meniscus near $y' = 0.95$, consequently forming a capillary ridge from surface tension-driven motion. Differently from the $Ma = 0$ case, the pressure (shown in Figure (11)) becomes more negative at the upper lid, as fluid drains out of the system from the positive flux (see Figure (12)) caused by our boundary conditions. The dynamic pressure-driven flow must counter the Marangoni and gravity-driven flows towards the lower lid in order to satisfy the zero surface velocity boundary condition at the upper lid. Solving the surface velocity boundary condition (III.21) for $\left(\frac{\partial p}{\partial y} + G\right)$, and substituting into the expression for the flux gives us

$$Q(L, t) = \frac{2h_g}{3} \frac{dL}{dt} + \epsilon Ma \frac{h_g^2}{6} \left(\frac{\partial \Gamma}{\partial y} \right).$$

Since $\frac{dL}{dt} = 0$, the flux at the upper lid is determined by the size of $\frac{\partial \Gamma}{\partial y}$.

The volume of tear fluid continues to grow and the tear film profile bulges at the lower meniscus, where the black line and capillary ridge formations occur but are now less pronounced at the lower lid when comparing to the $Ma = 0$ results. As a consequence, the global minimum is now in the black line near the upper lid. Capillarity and gravity collect lipid at the black line region within the lower meniscus at the beginning of the simulation, producing a strong Marangoni flow towards the lower lid. To satisfy the zero surface velocity boundary condition at the lower lid, the dynamic pressure-driven flow now must counter the large flow towards the lower lid. This results

in the tear fluid being pumped into the lower meniscus at a rate four times the size of the rate it is being drained from the system at the upper lid. As shown in Figure (11), the pressure is now high at the lower lid to produce the positive flux discussed above. Interestingly, this particular boundary condition configuration creates a self-driven pump of tear fluid at the lower lid.

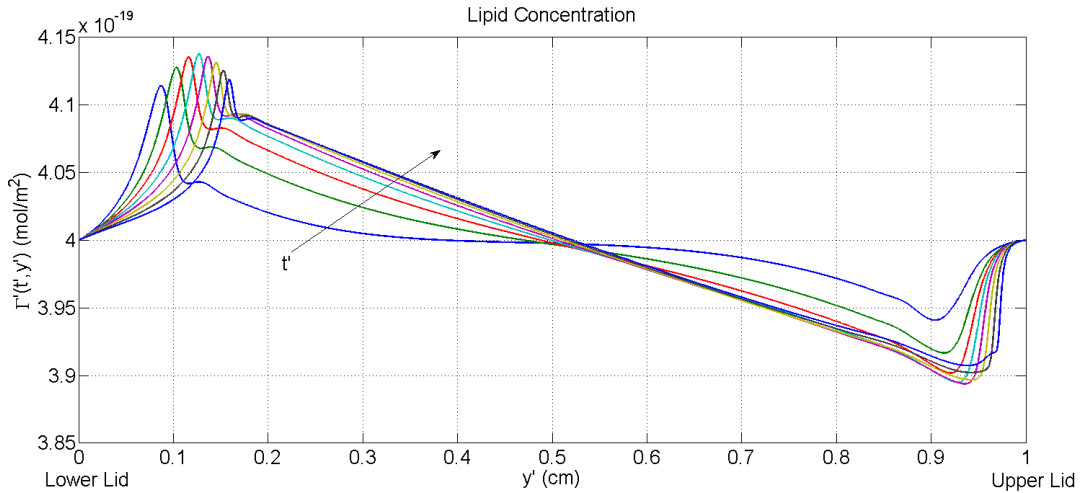


Figure 13: Evolution of the polar lipid concentration between $t' = 1.14\text{s}$ and $t' = 9.09\text{s}$ from equation (III.42).

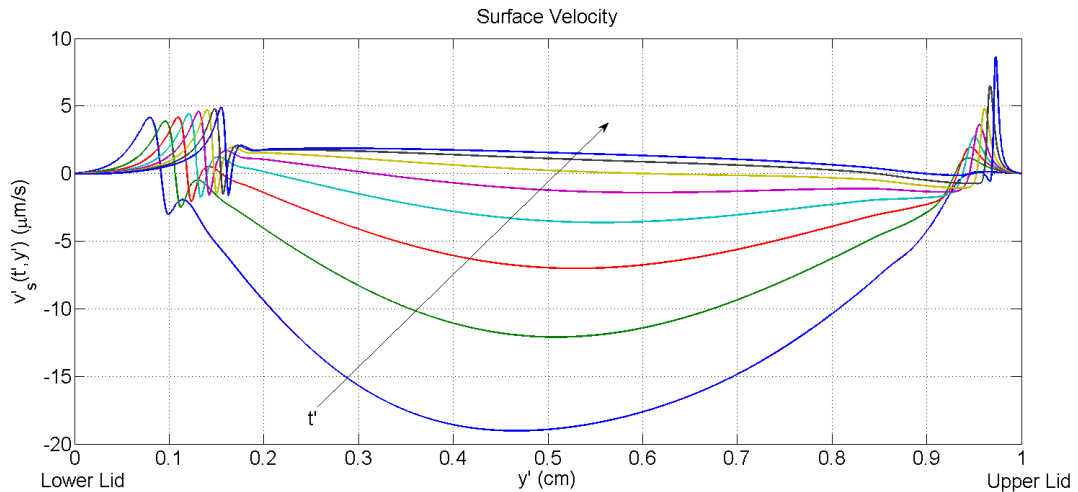


Figure 14: Surface velocity between $t' = 1.14\text{s}$ and $t' = 9.09\text{s}$ from equation (III.37).

Lipid dynamics are shown in Figure (13). Near the start of the simulation, the lipid is moved towards the lower lid across the domain, collecting at the lower lid black line. The surface velocity, shown in Figure (14), is initially negative in the center of the domain. Over time, as the lipid collects in the black line region, the Marangoni effect dominates the surface velocity between the

menisci to drive lipid towards the upper lid (similar to the upward drift seen experimentally). Additionally, Γ' appears to be evolving towards a steady state, since $\frac{\partial \Gamma}{\partial y} v_s + \Gamma \frac{\partial v_s}{\partial y} = 0$. Within the menisci, the Marangoni effect produces flows pointed towards the lower lid as described above.

V.1.3 Varying the Marangoni Number - Parameter Study

Several authors [2, 10, 14] used the value $\Gamma^* = 4 \times 10^{-7} \text{ mol/m}^2$ to express the dimensional quantity for lipid concentration on the tear film. This value was chosen because it was thought to appropriately represent what was calculated in previous research relating to surface tension gradients [6]. It is important to explore alternate values of Γ^* , and therefore alternate values of the Marangoni number in order to observe its influence on dynamics. The Marangoni number is involved in the governing equation for the change in tear film thickness (III.40), along with the governing equation for the change in lipid concentration (III.42). We explore the influence of the Marangoni number on the tear film at 3.3s.

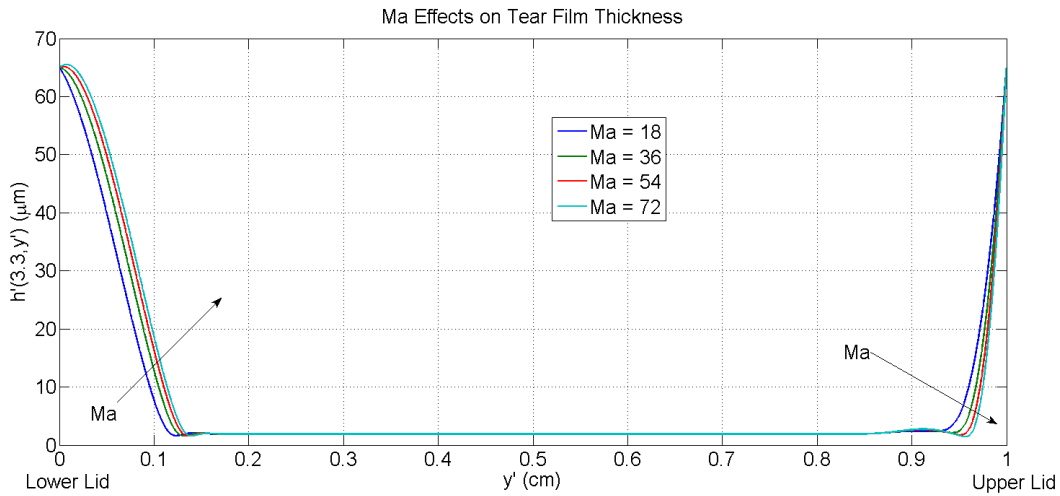


Figure 15: Influence of Ma on the aqueous layer evolution at $t' = 3.3s$ from equation (III.40).

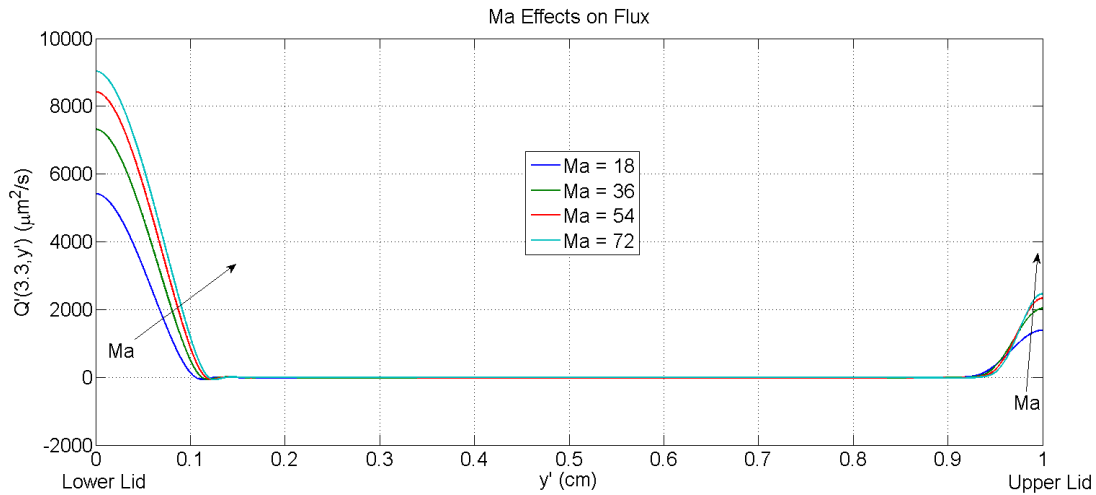


Figure 16: Influence of Ma on the aqueous flux at $t' = 3.3s$ from equation (III.38).

As the Marangoni number increases, the Marangoni flow becomes a more dominant effect in the dynamics. A large positive flux is required at the lower lid to compete with the larger Marangoni flux, causing fluid to enter the system through the lower lid. At the upper lid, fluid is drained from the system at a faster rate as the Marangoni number increases, as seen in Figure (15).

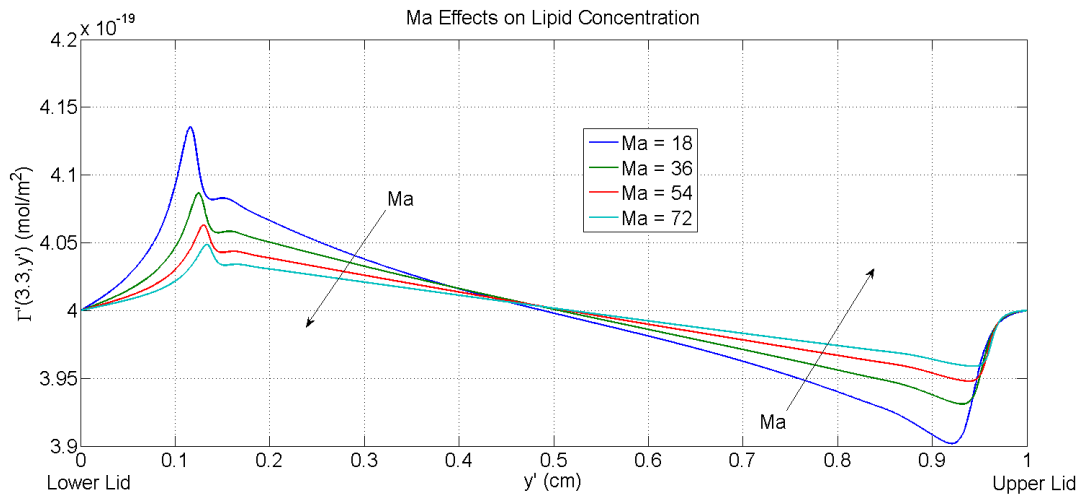


Figure 17: Influence of Ma on the polar lipid concentration evolution at $t' = 3.3s$ from equation (III.42).

The flux, plotted in Figure (16), has almost doubled in size in the menisci regions as the Marangoni number quadrupled. Dynamic pressure gradient flows at each lid must increase to compensate for the increased Marangoni flows, along with the flow driven by gravity to satisfy the zero surface velocity boundary condition. Black line formation then hastens at the menisci as the Marangoni

number increases.

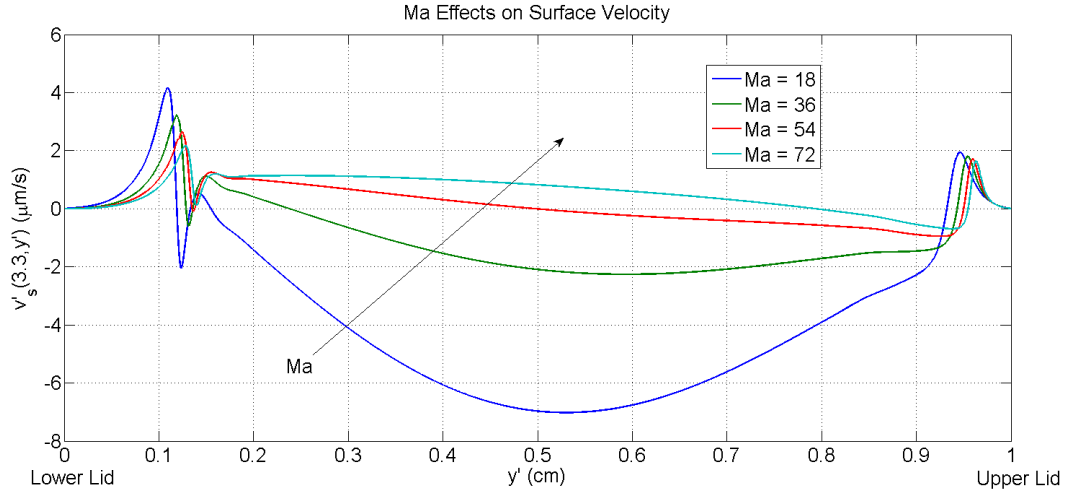


Figure 18: Influence of Ma on the surface velocity at $t' = 3.3s$ from equation (III.37).

The lipid concentration gradients across the domain become smaller (see Figure (17)), and the surface velocity is positive over more of the domain earlier in time for larger Marangoni numbers, as seen in Figure (18). Although the lipid concentration gradients decrease, the increasing Marangoni number amplifies the surface tension gradients, which dominate over the pressure gradients and gravity to produce a positive surface velocity across more of the domain.

V.2 Study of Tear Film Dynamics with Mixed Boundary Conditions

V.2.1 Mixed Boundary Condition

Running several simulations suggested that when B^* is close to zero, results similar to the specified lipid boundary condition will be produced. When B^* becomes large, results similar to the no lipid flux conditions will be produced, which will be presented in subsection V.2.2. The constant B for equations (III.19) and (III.18) was chosen such that $B^* = 1$. In the results presented below, the other boundary conditions, initial conditions, and parameter values are the same as Section V.1.2. Time spacing between each curve again is 1.136s.

Observing the tear film thickness during the 9.09 seconds of the evolution in Figure (19), we see less pooling in the lower meniscus and less draining in the upper meniscus. This can be seen by comparing the location of the black line regions in Figure (10) and Figure (19) as well as the value of the minimum tear film thickness in those regions.

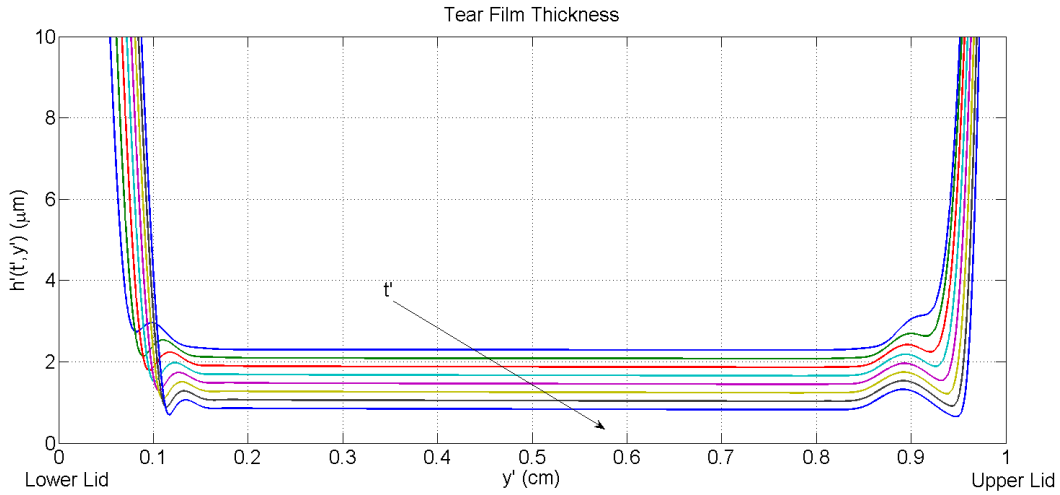


Figure 19: Aqueous layer between $t' = 1.14\text{s}$ and $t' = 9.09\text{s}$ when $B^* = 1$, from equation (III.40).

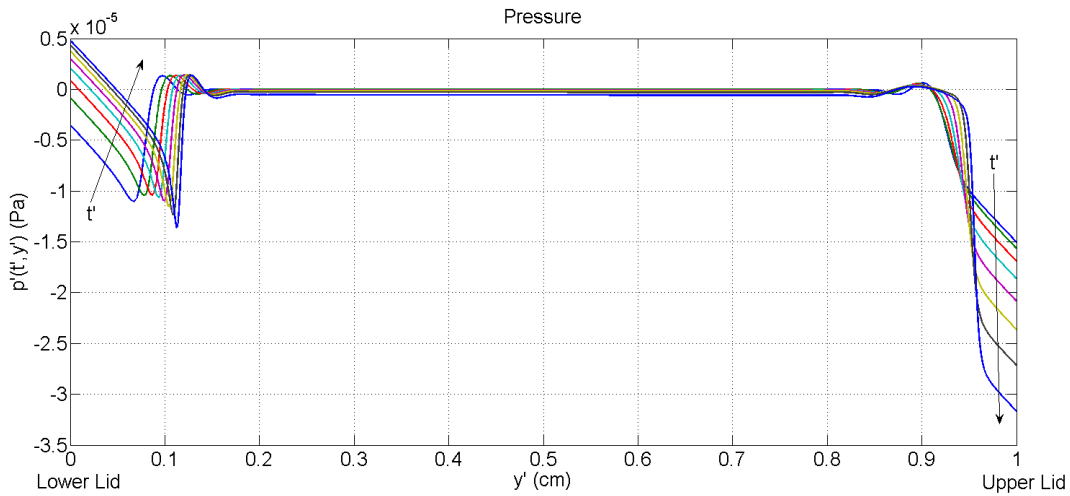


Figure 20: Pressure of the system between $t' = 1.14\text{s}$ and $t' = 9.09\text{s}$ when $B^* = 1$, from equation (III.41).

Figure (20) displays the evolution of pressure, where the curvature of the tear film causes the pressure to increase at the lower meniscus, and decrease at the upper meniscus. The values of the pressure are now smaller, as there is less curvature at the menisci. Similar to previous results, the pressure from the van der Waals force does not vary greatly between the menisci.

The flux produced from the utilization of the mixed boundary condition is displayed in Figure (21). Positive fluxes are half the size of the specified lipid boundary condition (compare with Figure (12)) within the menisci. Relaxing the control over the lipid at the boundaries allows smaller magnitude gradients as seen in Figure (22), where lipid at the boundaries does not greatly vary

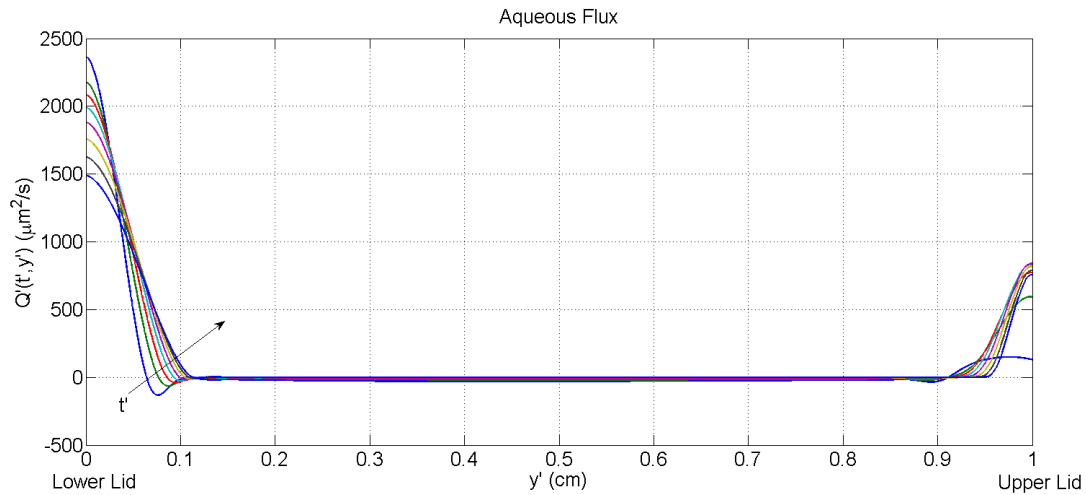


Figure 21: Aqueous flux between $t' = 1.14\text{s}$ and $t' = 9.09\text{s}$ when $B^* = 1$, from equation (III.38).

from the specified value of $4.0 \times 10^{-7} \text{mol/m}^2$. The smaller magnitude lipid gradients within the menisci regions produce a smaller Marangoni flow towards the lower lid. As a consequence, the dynamic pressure gradient needed to satisfy the zero surface velocity boundary condition at the lids is smaller, taming the positive aqueous flux at the lids.

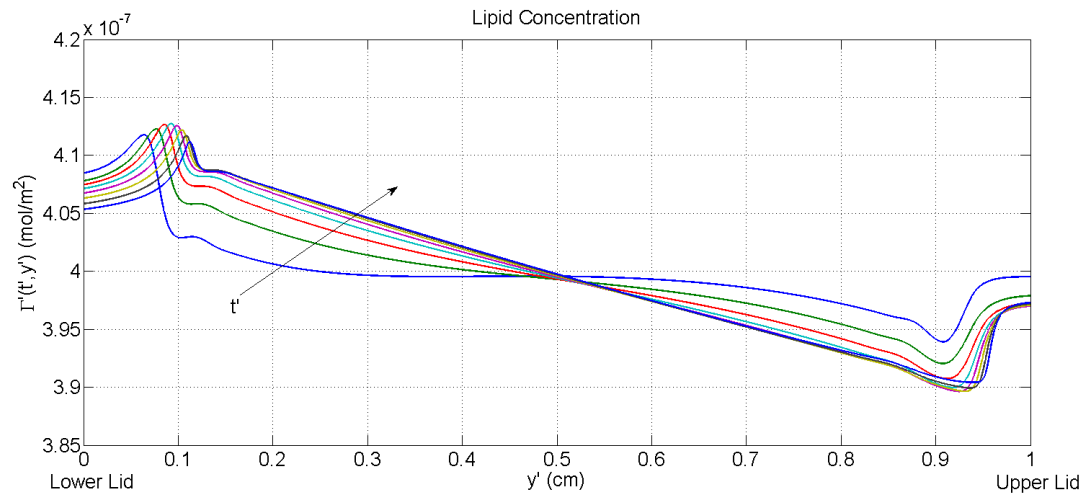


Figure 22: Evolution of the polar lipid concentration between $t' = 1.14\text{s}$ and $t' = 9.09\text{s}$ when $B^* = 1$, from equation (III.42).

Between the menisci, the lipid concentration is again larger near the lower meniscus than the upper, producing a positive surface tension gradient driving the Marangoni flow towards the upper lid. This Marangoni flow towards the upper lid competes with the gravity-driven flow.

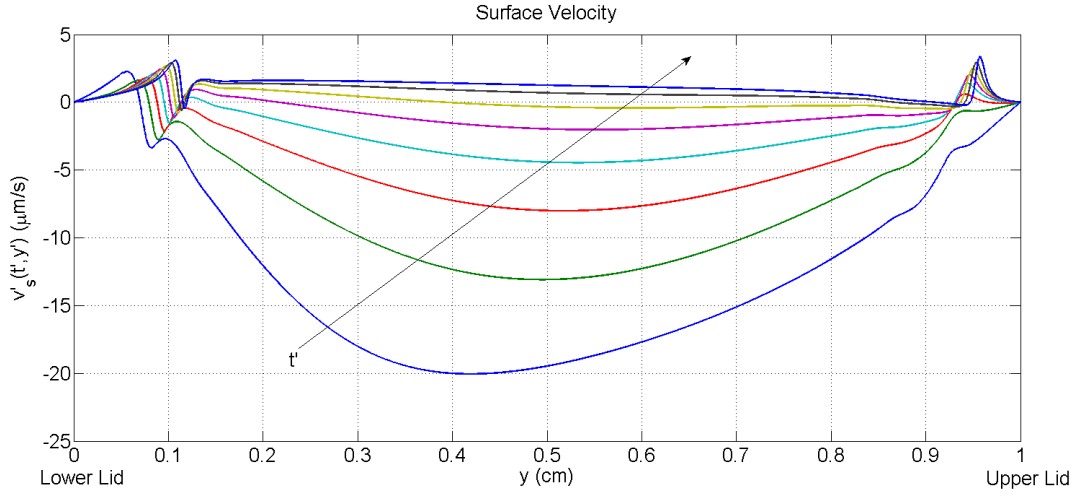


Figure 23: Surface velocity between $t' = 1.14\text{s}$ and $t' = 9.09\text{s}$ when $B^* = 1$, from equation (III.37).

As before, in the specified lipid boundary condition, the surface velocity (shown in Figure (23)) becomes positive in the center of the domain at the later times. Eventually, the Marangoni flow dominates the gravity-driven flow.

V.2.2 No Lipid Flux Boundary Condition

To ensure that the mixed boundary condition produced the results for no lipid flux, B^* was set to be 10^6 . Again, the other boundary conditions, initial conditions, and parameter values were kept the same, and the simulation was run for 9.09s with 1.136s between each curve.

The tear film profile (Figure (24)) remains relatively symmetric despite the influence of gravity and the Marangoni effect, where most fluid present in the system is located within the menisci. The black line region formation is similar to the specified lipid boundary condition with $Ma = 0$ when comparing Figure (4) and Figure (24).

Pressure profiles (shown in Figure (25)) do not vary greatly throughout time, determined by the curvature and tear film thickness, which do not greatly differ as time progresses. The dynamic pressure gradient at the menisci evolves towards $-G$, similarly to the specified lipid case with $Ma = 0$. Although the Marangoni flow can influence the aqueous dynamics, the lipid concentration does not greatly vary in the menisci.

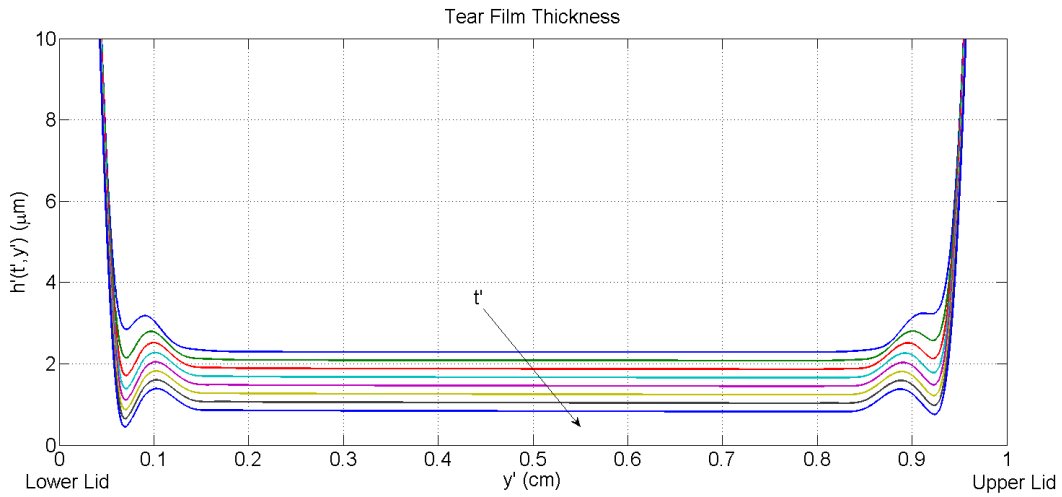


Figure 24: Aqueous layer between $t' = 1.14\text{s}$ and $t' = 9.09\text{s}$ when $B^* = 10^6$, from equation (III.40).

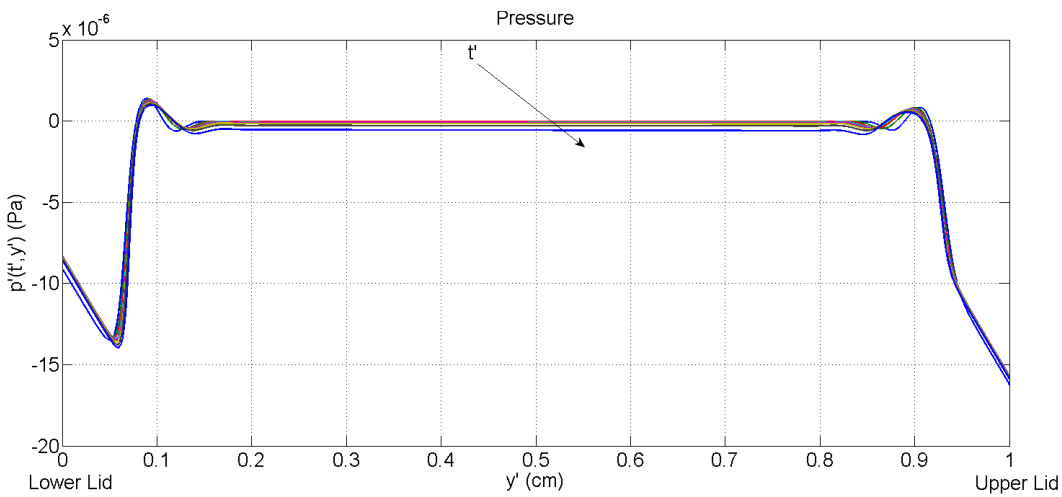


Figure 25: Pressure of the system between $t' = 1.14\text{s}$ and $t' = 9.09\text{s}$ when $B^* = 10^6$, from equation (III.41).

From the flux plots (Figure (26)), we observe that pressure gradients dominate within the menisci to cause fluid motion directed towards the lids, similar to when the Marangoni number was turned off for the specified lipid boundary condition. No aqueous flux at either lid occurs as a result from the combination of zero surface velocity, and no lipid flux boundary conditions.

Between the menisci, in the center of the domain, gravity causes a small flux towards the lower lid. Later in time, flux decreases in amplitude, and becomes closer to zero across the entire domain. This is because a Marangoni flow towards the upper lid is generated in the center of the domain that competes with the gravity-driven flow.

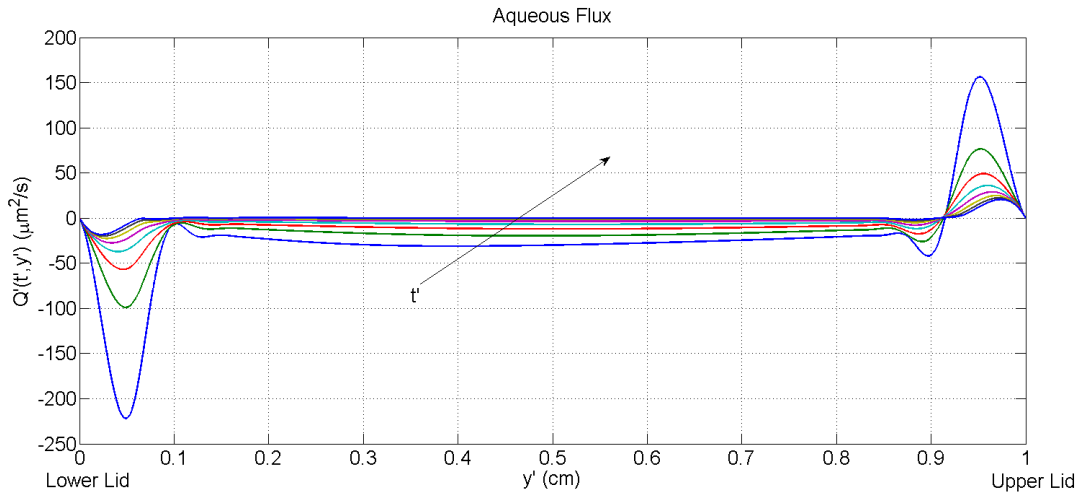


Figure 26: Aqueous flux between $t' = 1.14\text{s}$ and $t' = 9.09\text{s}$ when $B^* = 10^6$, from equation (III.38).

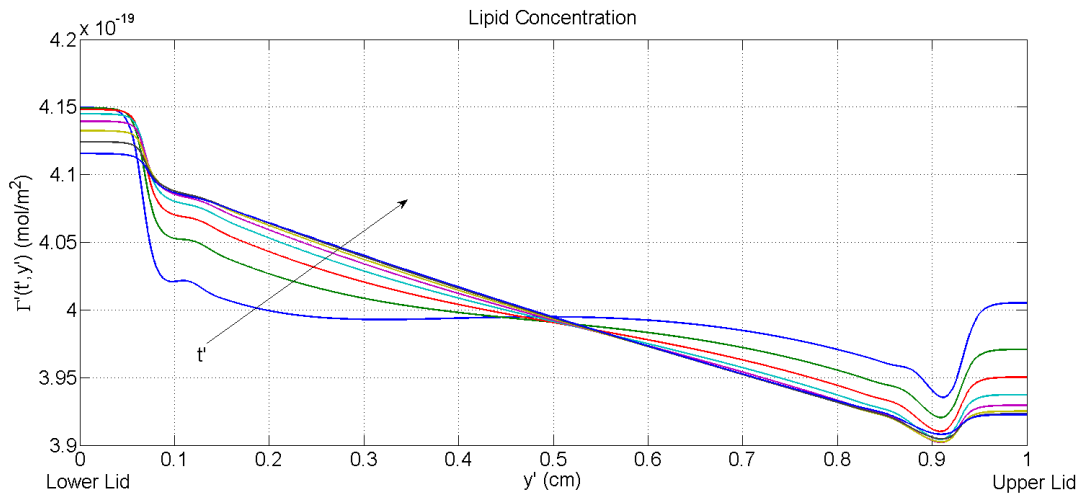


Figure 27: Evolution of the polar lipid concentration between $t' = 1.14\text{s}$ and $t' = 9.09\text{s}$ when $B^* = 10^6$, from equation (III.42).

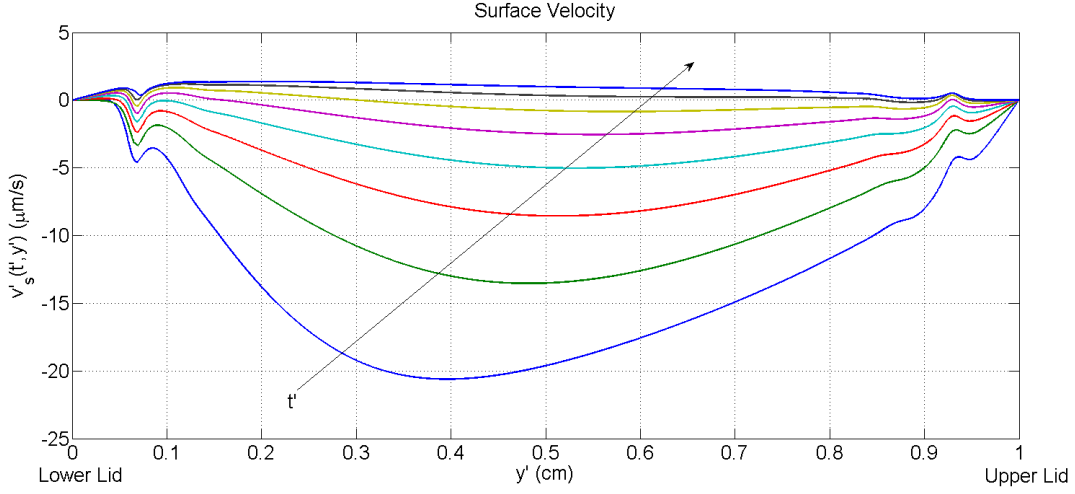


Figure 28: Surface velocity between $t' = 1.14\text{s}$ and $t' = 9.09\text{s}$ when $B^* = 10^6$, from equation (III.37).

The evolution of the lipid concentration is shown in Figure (27). The no-lipid-flux boundary conditions result in small lipid concentration gradients in the menisci and thus there is a very small Marangoni flow in the menisci regions. Between the menisci, a larger lipid concentration is located near the lower meniscus than the upper, producing a Marangoni flux towards the upper lid. The upward drift from the Marangoni flow in the center of the domain eventually dominates the gravity-driven flow as seen in the surface velocity plots in Figure (28). At the upper meniscus, the positive lipid gradient produces a surface tension-driven flux towards the lower lid.

VI. NUMERICAL SOLUTION - BLINKING EYE

In this section, we consider a partially blinking eye. The upper lid location, given by the function $y' = L'(t')$, now varies with time. We define our partial blink cycle as comprising of four different stages: opening phase, interblink period, closing phase, and a partially closed phase. In the opening phase, the upper lid opens up across $\frac{1}{4}$ of the ocular surface (from $y' = 0.75\text{cm}$ to $y' = 1\text{cm}$) in 0.51 seconds. For the interblink period, the eye remains open for 2.9 seconds ($y' = 1\text{cm}$). During the closing phase, the upper lid travels back down $\frac{1}{4}$ of the ocular surface from $y' = 1\text{cm}$ to $y' = 0.75\text{cm}$ in 0.51 seconds. The blink cycle ends with a partially shut phase where $y' = 0.75\text{cm}$ for 0.62 seconds. Figure(29) plots $L'(t')$. In comparison to a realistic partial blink, the opening and closing phases are longer, the interblink is shorter, and the partially shut phase is longer. Slowing down the blinking was necessary for the solution to integrate forward in time. Otherwise, the tear film would thin significantly causing the minimum thickness to go to

zero.

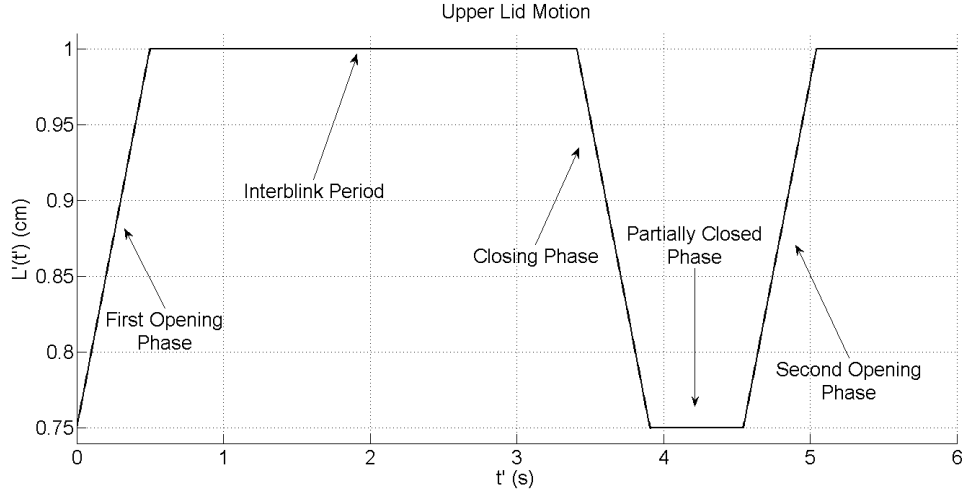


Figure 29: Plot capturing the motion of the upper lid over the duration of the simulation.

Beside the upper lid motion for previous simulations, we change the initial tear film profile so that $h'_{t_{yp}} = 5\mu\text{m}$ instead of $2.5\mu\text{m}$, and we used

$$\left. \frac{\partial \Gamma}{\partial y} \right|_{y=0} = \left. \frac{\partial \Gamma}{\partial y} \right|_{y=L} = 0$$

as the lipid boundary conditions. As a consequence, initially there is more tear volume and the lipid boundary conditions enforce a no diffusive flux condition. Furthermore, we can show that the amount of lipid in the system is conserved through the following area calculation by first rewriting equation (III.42)

$$\frac{\partial \Gamma}{\partial t} + \frac{\partial}{\partial y} Q_{\Gamma} = 0, \quad (\text{VI.1})$$

where Q_{Γ} is the nondimensionalized lipid flux, and integrating equation (VI.1) with respect to y . Using Leibniz's rule, we find that

$$\frac{\partial}{\partial t} \int_0^{L(t)} \Gamma \partial y = \int_0^{L(t)} \frac{\partial \Gamma}{\partial t} \partial y + \Gamma(t, L(t)) \frac{dL}{dt},$$

which we substitute back into the integrated equation (VI.1) to obtain

$$\frac{\partial}{\partial t} \int_0^{L(t)} \Gamma \partial y = \Gamma(t, L(t)) \frac{dL}{dt} - Q_{\Gamma}(t, L(t)) + Q_{\Gamma}(t, 0),$$

and since the lipid flux $Q_{\Gamma}(t, L(t)) = \Gamma(t, L(t)) \frac{dL}{dt}$ at the upper lid, and $Q_{\Gamma}(t, 0) = 0$ at the lower lid due to our boundary conditions, the lipid initially present in the system is conserved, as

$$\frac{\partial}{\partial t} \int_0^{L(t)} \Gamma \partial y = 0.$$

VI.1 First Opening Phase

We begin by exploring the initial opening phase of the lid motion in Figure (30). Recall, when we enforce the surface velocity of the aqueous layer to match the lid speed, the flux at the upper lid is given by

$$Q(L, t) = \frac{2h_g}{3} \frac{dL}{dt} + \epsilon Ma \frac{h_g^2}{6} \frac{\partial \Gamma}{\partial y} \Big|_{y=L}.$$

With the no diffusive flux lipid boundary condition, the flux is proportional to the lid motion. Note that this lipid flux boundary condition has been previously studied [14].

At the upper lid, the tear film bulges due to the flux induced by the lid motion. Pressure changes near the upper lid according to the curvature of the tear film formed by the lid motion. Capillarity dominates at the upper lid to produce a large positive flux. The positive flux from capillarity and the Marangoni effect competes with gravity to create a bulge at the upper meniscus until the upper lid reaches the maximum length of 1cm. Near the stationary lower lid, the meniscus-induced-thinning is apparent as no tear fluid enters the system. Recall that we do not control the aqueous flux as boundary conditions in contrast to previously studied models.

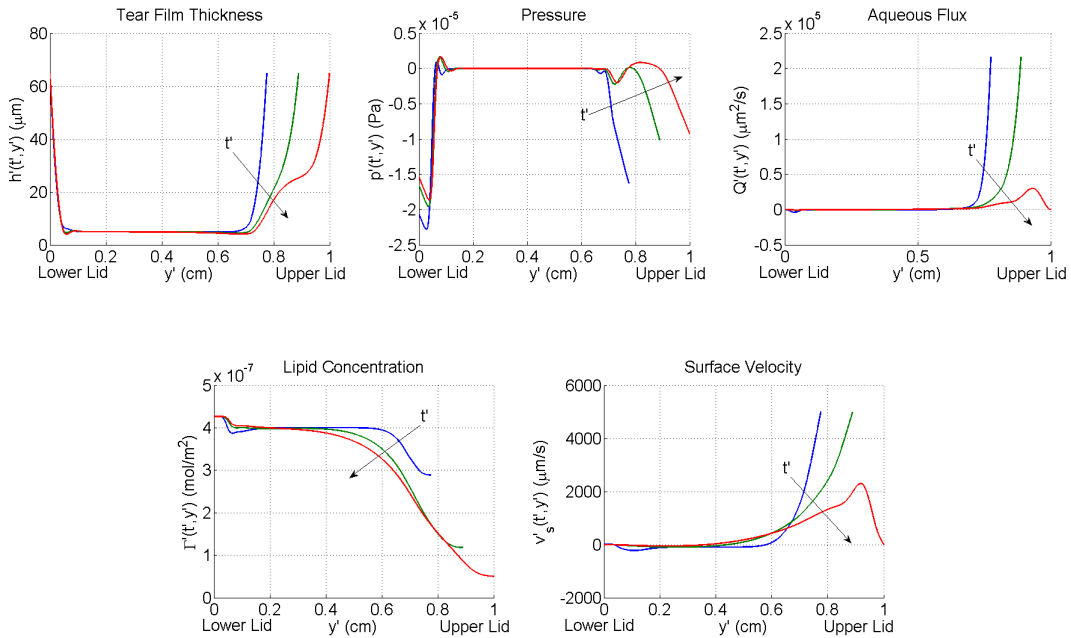


Figure 30: Tear film dynamics during the initial opening phase of the blink at $t' = 0.057s$, $t' = 0.227s$, and $t' = 0.511s$.

Flux is zero at the lower lid due to the no diffusive lipid flux and zero surface velocity boundary conditions, where the slightly negative flow within the lower meniscus contributes to the formation of the black line. Lipid concentration forms a negative gradient across the domain due to the surface velocity, inducing surface tension-driven Marangoni flux towards the upper lid. Next we observe the interblink period, where we allow the tear dynamics to evolve for 2.9s.

VI.2 Interblink Period

As a consequence of the blink, the tear film evolution in the upper meniscus is different from our previous open eye calculation (compare Figure (31) with Figures (10), (19), and (24)). During the interblink period, the tear fluid in the upper meniscus is now traveling towards the lower lids. The gravity-driven flow now dominates over the weaker meniscus-induced flow. In addition, the formation of a ridge produces curvature influencing the change in pressure at the upper meniscus to result in a larger negative flux later in time, as shown in Figure (33). Time spacing between each line is 0.568 seconds.

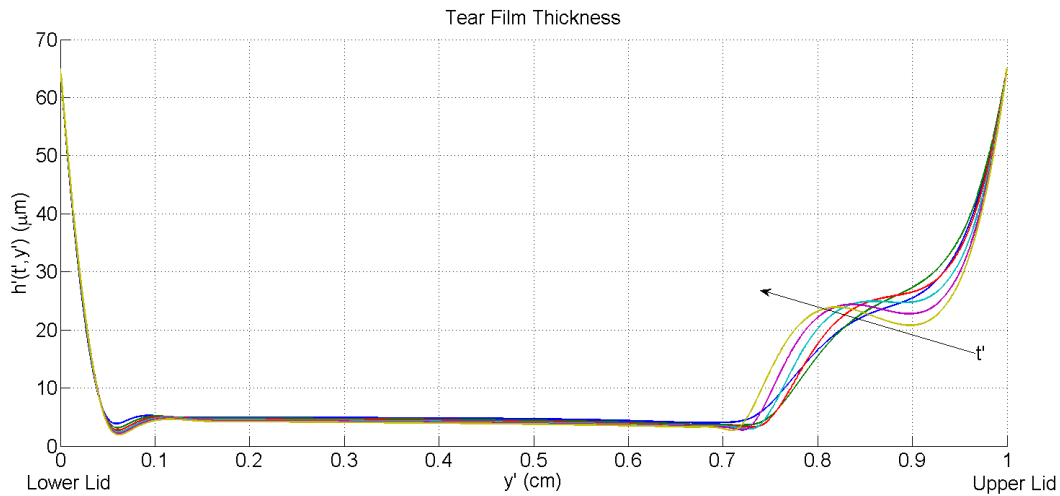


Figure 31: Aqueous layer evolution over 2.9s post-blink from equation (III.40).

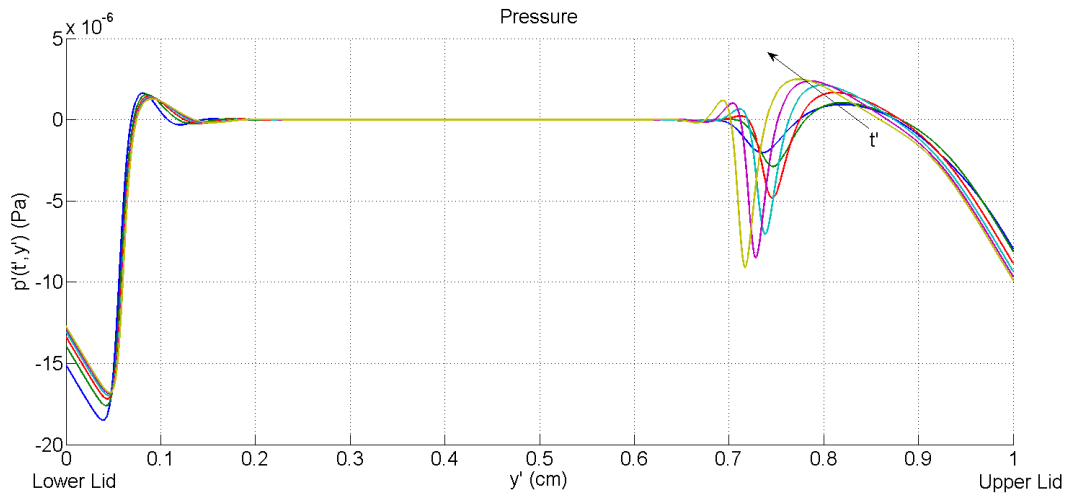


Figure 32: Pressure of the system over 2.9s post-blink from equation (III.41).

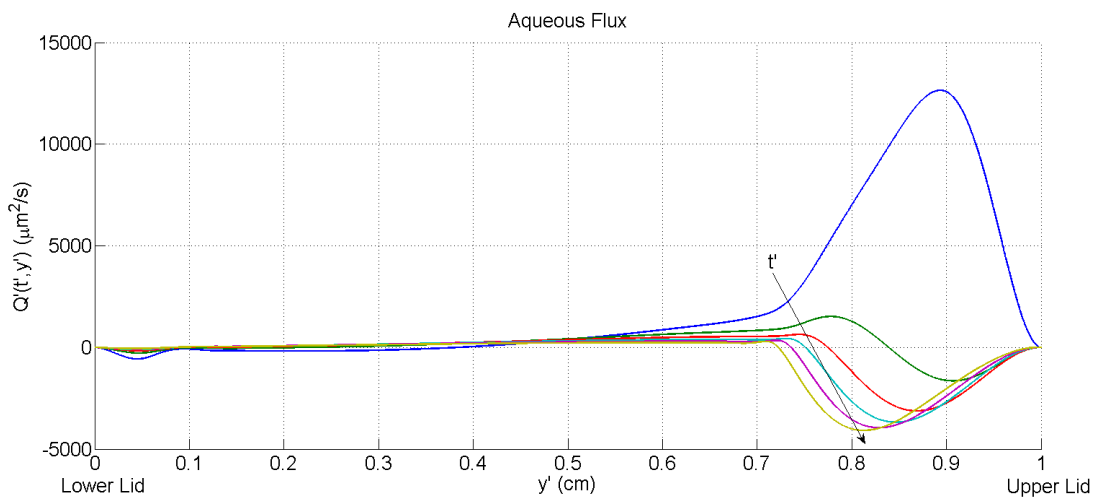


Figure 33: Aqueous flux over 2.9s post-blink from equation (III.38).

Surface tension gradients dominate the fluid flow between the menisci due to the strictly negative slope of the lipid concentration profile (Figure (34)), causing a Marangoni flux towards the upper lid (Figure (35)). Consequently, the Marangoni effect produces a positive flux later in time, indicating upward drift of the lipid. Continuing with the study, we initiate a blink with downward motion of the upper lid.

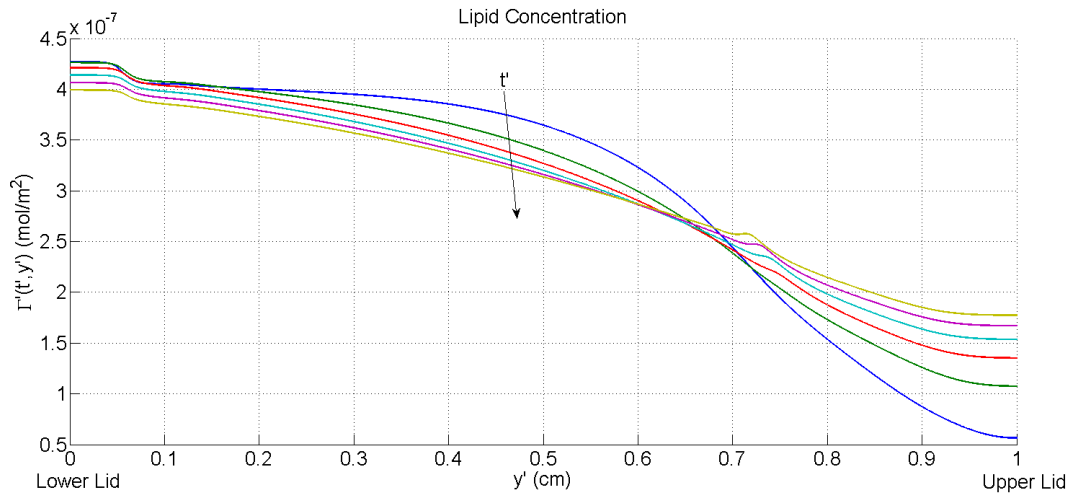


Figure 34: Evolution of the polar lipid concentration over 2.9s post-blink from equation (III.42).

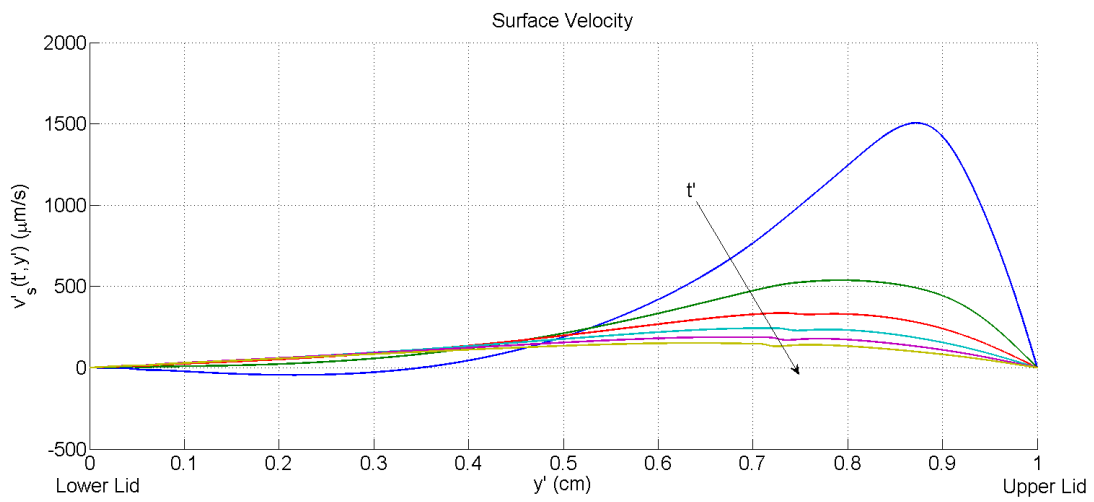


Figure 35: Surface velocity over 2.9s post-blink from equation (III.37).

VI.3 Closing Phase

The aqueous fluid near the upper meniscus is drained out of the system through the upper lid, induced by the lid motion (Figure (36)). Fluid near the upper lid still bulges throughout the closing cycle, although the bulge is shifted towards the lower lid due to gravity and the Marangoni effect. Large changes in pressure are observed due to the changing curvature of the aqueous layer from the bulge in the tear film thickness. The pressure gradients compete with gravity and the Marangoni flux, along with the downward motion of the lid to produce the negative flux near the upper lid. Lipid concentration maintains a negative gradient until reaching the upper meniscus. Surface-tension-induced fluxes point towards the upper lid everywhere except within the upper meniscus, where the large positive slope of the lipid concentration produces a negative Marangoni flux and surface velocity.

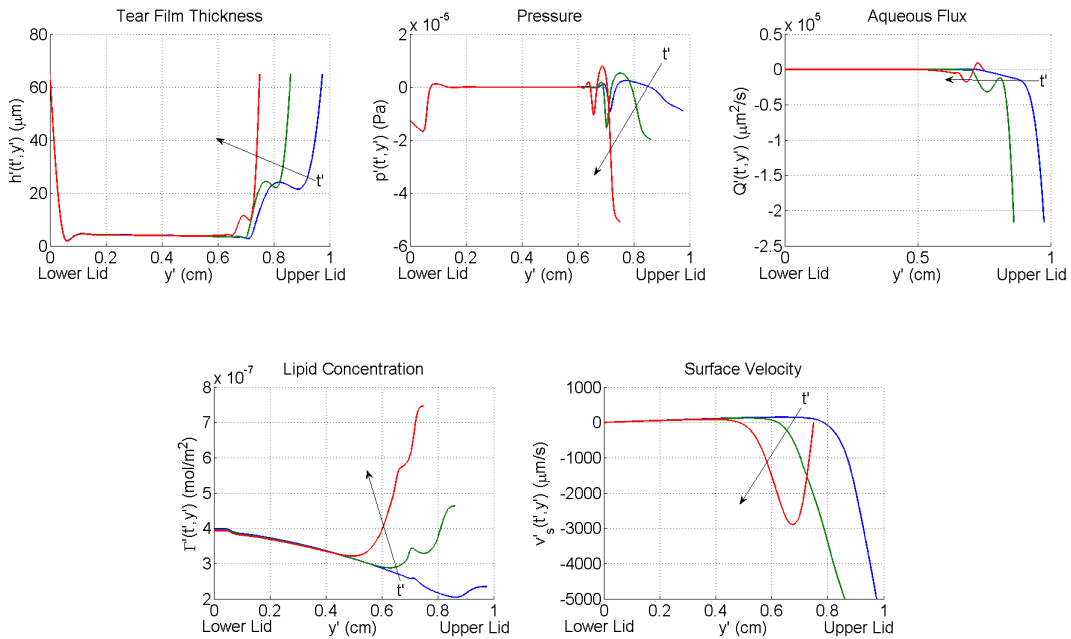


Figure 36: Tear film dynamics during the closing phase of the blink at $t' = 3.468\text{s}$, $t' = 3.638\text{s}$, and $t' = 3.922\text{s}$ after the interblink period.

VI.4 Partially Closed Phase

Recall that in our blink cycle the lid stays stationary for a short time between the closing and opening phases. The time between the closing and opening phase results in thinning of the tear film due to evaporation, noticeably at the ridge within the upper meniscus (Figure (37)). Flux is then influenced by the thinning ridges. Within the 0.62s period between lid motion, the flux and surface velocity tend towards zero across the domain, and the lipid concentration advects, producing smaller gradients and reducing the Marangoni flux. Near the upper lid, capillarity dominates the flux, and the Marangoni effect dominates surface velocity.

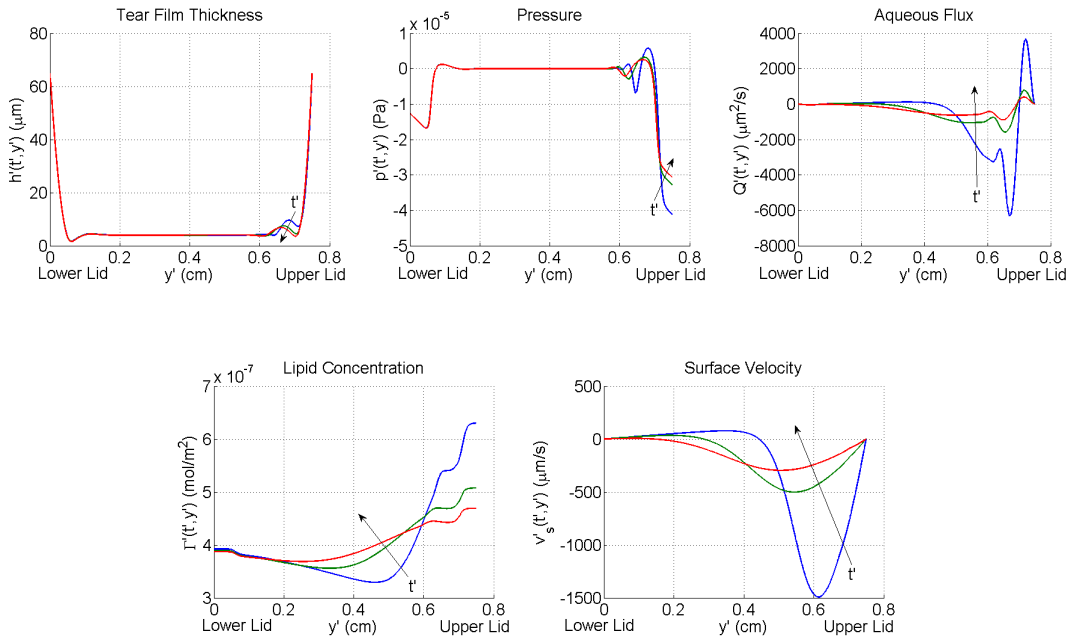


Figure 37: Tear film dynamics between the closing and opening phase of the blink at $t' = 3.979s$, $t' = 4.206s$, and $t' = 4.542s$ after the closing phase.

VI.5 Second Opening Phase

Results of the second opening phase are similar to that of the initial opening phase. Differently, the bulge formed from the first opening phase in the aqueous layer is apparent throughout the lid motion, influencing the change in pressure and the flux near the upper meniscus as another capillary ridge begins to form, as seen in Figure (38). Changes in pressure form to compensate for all ridges near the upper meniscus, and is added to the positive surface-tension-induced Marangoni flux to produce a dominantly positive aqueous flux until the eye is completely open. As the lid opens, the profile of the lipid concentration forms a negative gradient across the domain, again producing a positive Marangoni flux, which also contributes to the positive surface velocity.

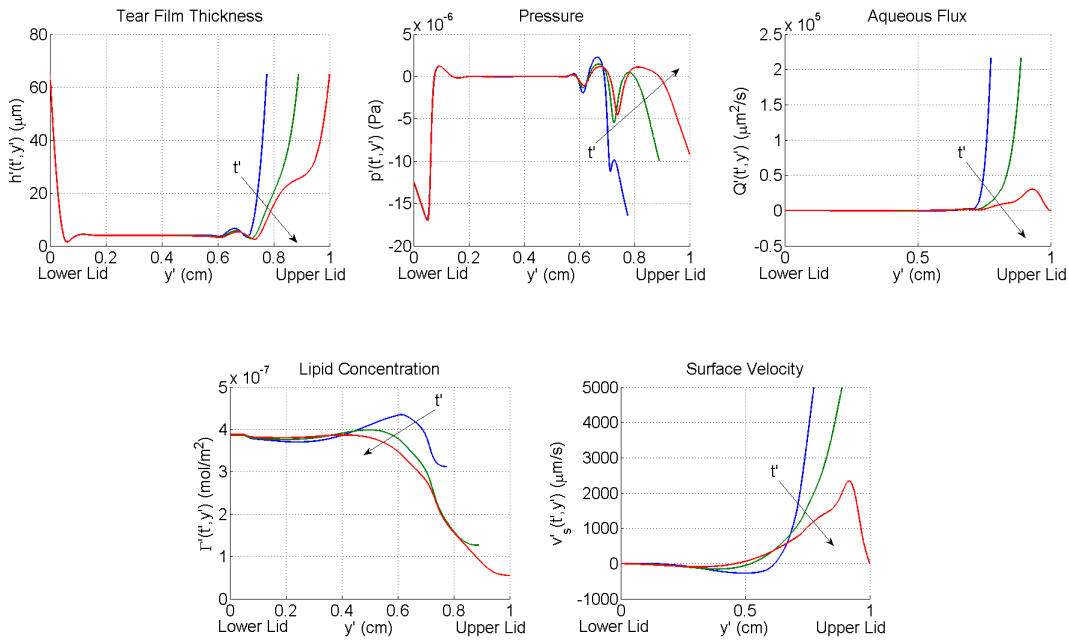


Figure 38: Tear film dynamics during the opening phase of the blink at $t' = 4.599\text{s}$, $t' = 4.819\text{s}$, and $t' = 5.053\text{s}$ after the partially closed phase.

VII. DISCUSSION

VII.1 Discussion and Conclusion

The goal of this work was to determine if specifying the lipid at the lids in the mathematical model would be sufficient in capturing the physiological lipid reservoir seen in Figure (1). In the absence of the Marangoni effect ($Ma = 0$), we found the evolution of the tear film thickness on the open eye to be qualitatively the same as the prior works [2, 5, 10, 14]. With the Marangoni effect (Ma nonzero), the coupled system was found to be highly sensitive to the choice of lipid boundary conditions. We explored the influences of specified lipid, mixed lipid, and no lipid flux boundary conditions while controlling the surface velocity at the lids.

We found the specified lipid boundary condition, mimicking a lipid reservoir, created large positive fluxes at the lids pumping aqueous tear fluid into and out of the system. By specifying the lipid concentration at the lids, Marangoni flows were established within the menisci, which were countered by dynamic-pressure-gradients to pump fluid into the system at the lower lid and out of the system through the upper lid, to generate a zero surface velocity. This aqueous flux at the lids is not present in prior modeling efforts, due to all prior works choosing to control the aqueous flux as a boundary condition.

Using the mixed lipid boundary condition relaxed the lipid concentration gradients at the menisci, while not greatly varying the lipid concentration at the lids to produce results for a less controlled lipid reservoir. The large positive flux produced by the specified lipid boundary condition at the lower lid was alleviated, and the surface velocity did not vary greatly across the domain as a result.

Lastly, the no lipid flux boundary condition produced a symmetric like tear film profile throughout the simulation when comparing to the specified lipid and mixed lipid boundary conditions. Symmetry of the tear film is a result of a lacking aqueous flux occurring at the lids produced by the relationship between the zero surface velocity and zero lipid flux boundary conditions. Since the Marangoni effect was present in the simulation, the profile for the surface velocity is similar to the other explored boundary conditions, but the smaller lipid concentration gradients produced a smaller Marangoni flux for the capillary driven flux to compete with at the menisci, resulting in a less positive surface velocity.

For the specified lipid boundary condition, we found that increasing the Marangoni number

through the increasing of the lipid concentration across the domain caused more upward drift of the lipid, consistent with experiment and other mathematical models. Furthermore, the lipid concentration is highly mobile within the first second of the simulations, and drifts upward later in time for all choices of boundary condition. The black line formation is slightly slower in the model than in reality for all explored boundary conditions. Due to the difficulties in imaging the tear film dynamics at the lids, the proper choice for set of boundary conditions we explored remains unclear. We understand that there is not an unlimited supply of aqueous fluid beneath the lids, so the specified lipid boundary condition may not necessarily be realistic for the open eye.

Results for the blinking eye were found to be sensitive to the aqueous flux at the boundary. Specifically, we were not able to run a complete simulation of the open phase of the blink cycle with either the specified lipid boundary condition or the mixed lipid boundary condition. In these cases, too much aqueous fluid is pumped out of the system at the upper lid causing the tear film to thin rapidly and break up. These results suggest the need to control the aqueous flux at the boundary but more exploration is needed.

VII.2 Future Work

As seen in this thesis, the boundary conditions have a drastic effect on the evolution of the tear film. To work towards a complete understanding of the tear film model, more boundary conditions need to be explored. In this thesis, we introduced a mixed lipid boundary condition, which allowed us to explore both a specified lipid boundary condition, and no lipid flux boundary condition as well. Further work is needed to understand how this mixed lipid boundary condition influences the dynamics during the blink cycle. In addition, in this thesis, for the aqueous evolution equation, we chose to control the surface velocity and pin the tear film thickness at the lids. As discussed in the literature review, most prior works control the aqueous flux into the system and pin the tear film thickness. Therefore, it would be interesting to explore a mixed aqueous boundary condition including the surface velocity and aqueous flux.

At the end of the simulations where mixed lipid boundary conditions are applied, $\epsilon \frac{\partial h}{\partial y}$ is approximately 0.28 in the upper meniscus. Considering the large slopes of the tear film profile and generally large gradients near the menisci, we cannot ensure that lubrication theory is valid from our solutions. Prior literature has also raised concerns about the validity of lubrication theory. An option to progress would be to regard the terms including epsilon as large to solve

the incompressible Navier-Stokes model without removing terms, similar to work by Zubkov [29], but using our boundary conditions for the open eye. Zubkov found that differences occur within the menisci, where the directions of flow differ in the lubrication model compared with flows predicted from the incompressible Navier-Stokes equations [29]. Including all terms of the Navier-Stokes would require a more robust code, and the results would be complex.

Lipid concentration profiles of our solutions (seen in Figures (13), (22), and (27)) hint at the presence of a boundary layer-type structure, where much of the solution response structure lies in the vicinity of the domain edges. Performing a study on these regions will elucidate the complex solutions found within the menisci for all choices of boundary conditions in this thesis. From the analysis, it may be possible to identify an underlying similarity solution structure, since many solution profiles appear to have a self similar character. This local analysis is necessary to understand the physics occurring within the menisci, but also may lead to a solution whose limit may allow us to identify self-consistent boundary conditions on the lubrication flow (via asymptotic matching), valid away from these edge regions.

VIII. ACKNOWLEDGMENT

This material is based upon work supported by the National Science Foundation under Grant Number (1412141). Any opinions, findings, and conclusions or recommendations expressed in this material are those of the author(s) and do not necessarily reflect the views of the National Science Foundation.

IX. APPENDIX

Rochester Institute of Technology Mail GREGORY BARRON <gab1232@g.rit.edu>

Picture for thesis

2 messages

Gregory Barron (RIT Student) <gab1232@rit.edu>Tue, Aug 25, 2015 at 7:45 AM

To: king-smith.1@osu.edu

Dr. King-Smith,

This is Greg, one of Dr. Maki's students studying tear film dynamics - we ended up meeting at the ARVO eye conference this year.

I was wondering if you would be willing to allow me to use picture 5b (in your attached paper below) in my master's thesis on tear film dynamics. The picture hints towards a lipid reservoir, and it would help the reader understand what I'm trying to capture with my math model. It would really tie together my introduction.

Thanks for your time,
-Greg

KingSmithEtal_IOVS09_lipidmovemt(2).pdf

410K

King-Smith, Peter <king-smith.1@osu.edu>Tue, Aug 25, 2015 at 8:51 AM

To: "Gregory Barron (RIT Student)" <gab1232@rit.edu>

Cc: "King-Smith, Peter" <king-smith.1@osu.edu>

Good to hear from you! Yes, you are welcome to use the figure.

Best wishes,

Ewen

From: Gregory Barron (RIT Student) [gab1232@rit.edu]

Sent: Tuesday, August 25, 2015 7:45 AM

To: King-Smith, Peter

Subject: Picture for thesis

[Quoted text hidden]

REFERENCES

- [1] VS Ajaev and GM Homsy. Steady vapor bubbles in rectangular microchannels. *Journal of Colloid and Interface Science*, 240(1):259–271, 2001.
- [2] E Aydemir, CJW Breward, and TP Witelski. The effect of polar lipids on tear film dynamics. *Bulletin of Mathematical Biology*, 73(6):1171–1201, 2011.
- [3] RE Berger and S Corrsin. A surface tension gradient mechanism for driving the pre-corneal tear film after a blink. *Journal of Biomechanics*, 7(3):225–238, 1974.
- [4] RJ Braun. Dynamics of the tear film. *Annual Review of Fluid Mechanics*, 44:267–297, 2012.
- [5] RJ Braun and AD Fitt. Modelling drainage of the precorneal tear film after a blink. *Mathematical Medicine and Biology*, 20(1):1–28, 2003.
- [6] CJW Breward, RC Darton, PD Howell, and JR Ockendon. The effect of surfactants on expanding free surfaces. *Chemical Engineering Science*, 56(8):2867–2878, 2001.
- [7] AJ Bron, JM Tiffany, SM Gouveia, N Yokoi, and LW Voon. Functional aspects of the tear film lipid layer. *Experimental Eye Research*, 78(3):347–360, 2004.
- [8] RS Burdon. *Surface tension and the spreading of liquids*. CUP Archive, 1949.
- [9] G Chesshire and WD Henshaw. Composite overlapping meshes for the solution of partial differential equations. *Journal of Computational Physics*, 90(1):1–64, 1990.
- [10] Q Deng. *Tear film modeling in 1D and 2D moving geometry with high-order methods*. University of Delaware, 2013.
- [11] MG Doane. Blinking and the mechanics of the lacrimal drainage system. *Ophthalmology*, 88(8):844–851, 1981.
- [12] FJ Holly and MA Lemp. Tear physiology and dry eyes. *Survey of Ophthalmology*, 22(2):69–87, 1977.
- [13] AS Janine. The epidemiology of dry eye disease: report of the epidemiological subcommittee of the international dry eye workshop. *Ocul Surf*, 5(2):93–107, 2007.
- [14] MB Jones, DLS McElwain, GR Fulford, MJ Collins, and AP Roberts. The effect of the lipid layer on tear film behaviour. *Bulletin of Mathematical Biology*, 68(6):1355–1381, 2006.

-
- [15] PE King-Smith, BA Fink, JJ Nichols, KK Nichols, RJ Braun, and GB McFadden. The contribution of lipid layer movement to tear film thinning and breakup. *Investigative Ophthalmology & Visual Science*, 50(6):2747–2756, 2009.
- [16] PE King-Smith, JJ Nichols, KK Nichols, BA Fink, and RJ Braun. Contributions of evaporation and other mechanisms to tear film thinning and break-up. *Optometry & Vision Science*, 85(8):623–630, 2008.
- [17] MA Lemp, C Baudouin, J Baum, et al. The definition and classification of dry eye disease: Report of the definition and classification subcommittee of the international dry eye workshop. *Ocul Surf*, 5(2):B75–92, 2007.
- [18] JC Mainstone, AS Bruce, and TR Golding. Tear meniscus measurement in the diagnosis of dry eye. *Current Eye Research*, 15(6):653–661, 1996.
- [19] KL Maki, RJ Braun, P Ucciferro, WD Henshaw, and PE King-Smith. Tear film dynamics on an eye-shaped domain. part 2. flux boundary conditions. *Journal of Fluid Mechanics*, 647:361–390, 2010.
- [20] WD Mathers and TE Daley. Tear flow and evaporation in patients with and without dry eye. *Ophthalmology*, 103(4):664–669, 1996.
- [21] KL Miller, KA Polse, and CJ Radke. Black-line formation and the "perched" human tear film. *Current Eye Research*, 25(3):155–162, 2002.
- [22] A Oron, SH Davis, and SG Bankoff. Long-scale evolution of thin liquid films. *Reviews of Modern Physics*, 69(3):931, 1997.
- [23] AD Pucker and KM Haworth. The presence and significance of polar meibum and tear lipids. *The Ocular Surface*, 13(1):26–42, 2015.
- [24] EK Sakata and JC Berg. Surface diffusion in monolayers. *Industrial & Engineering Chemistry Fundamentals*, 8(3):570–575, 1969.
- [25] A Sharma, S Tiwari, R Khanna, and JM Tiffany. Hydrodynamics of meniscus-induced thinning of the tear film. In *Lacrimal Gland, Tear Film, and Dry Eye Syndromes 2*, pages 425–431. Springer, 1998.
- [26] HA Stone. A simple derivation of the time-dependent convective-diffusion equation for surfactant transport along a deforming interface. *Physics of Fluids A: Fluid Dynamics (1989-1993)*, 2(1):111–112, 1990.

-
- [27] KN Winter, DM Anderson, and RJ Braun. A model for wetting and evaporation of a post-blink precorneal tear film. *Mathematical Medicine and Biology*, page dqp019, 2009.
- [28] H Wong, I Fatt, and CJ Radke. Deposition and thinning of the human tear film. *Journal of Colloid and Interface Science*, 184(1):44–51, 1996.
- [29] VS Zubkov, CJW Breward, and EA Gaffney. Meniscal tear film fluid dynamics near marx’s line. *Bulletin of Mathematical Biology*, 75(9):1524–1543, 2013.